SOME EFFECTS OF THE STRESS STATE ON THE DEFORMATION AND FRACTURE OF A MEDIUM CARBON STEEL

by H.D. Chandler

The thesis is submitted in partial
fulfilment of the requirements for
the degree of M.Sc. in Materials Science
at the University of Glasgow

ProQuest LLC.
789 East Eisenhower Parkway
P.O. Box 1346
Ann Arbor, MI 48106 – 1346

FIG A

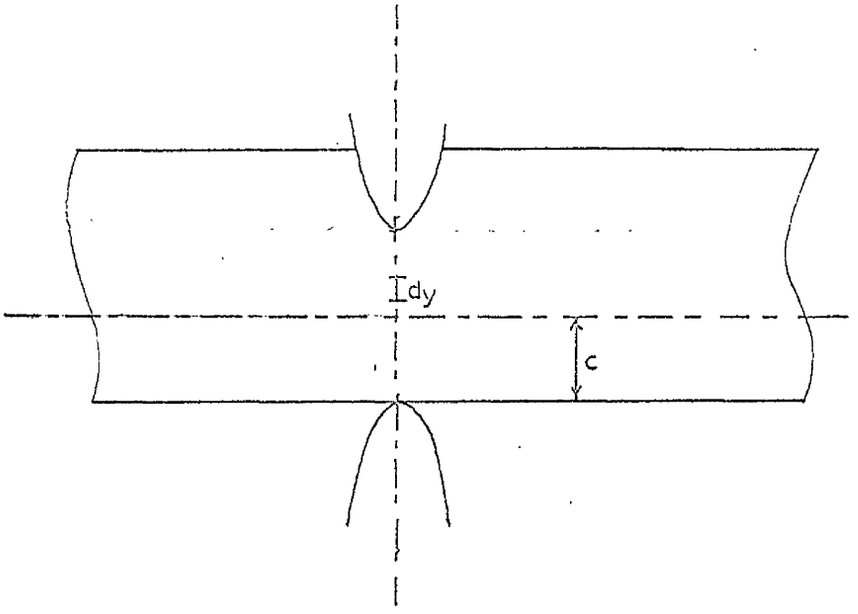

FIG B

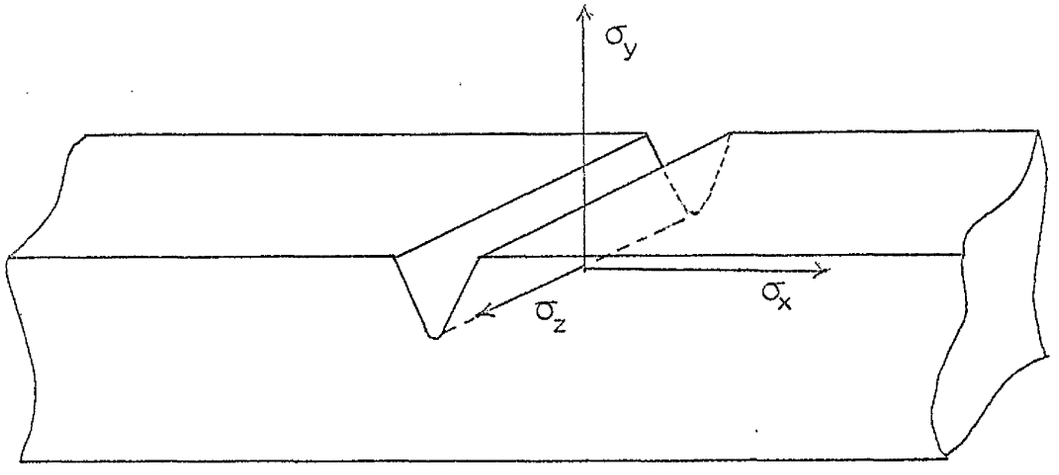

Acnowledgements

The author wishes to thank Dr. A.C. Mackenzie and Dr. P.Hancock of the department of Mechanics and Mechanisms at the University of Glasgow for their helpful discussions and advice during the course of this work.

Thanks are also due to the technical staff of the above department for the preparation of specimens etc.

CONTENTS

Chapter 1

INTRODUCTION

The aim of this work was to investigate the effect of the stress state on the mechanical behaviour of a medium carbon steel and to relate this to structural changes that take place.

An early reference to strain induced damage in carbon steels was by Jenkins who noticed cracks across the pearlite lamellae in the neigbourhood of fracture surfaces of tensile test pieces (1). These were found at temperatures mostly below 250 deg. C and at angles of about 45 deg. to the tensile axis.

Danko and Stout (2) carried out Charpy tests on eutectoid composition steel and found that pearlite deformation occurred by kinking of the lamellae, some of the kinks being sharp enough to cause cracking. The kinks became sharper as the interlamellar spacing decreased. The deformation of the cementite, a usually brittle material is attributed to the presence of a local hydrostatic pressure preventing cracking.

Puttick (3) found in a tensile specimen of eutectoid steel that deformation occurred by slip parallel to the

lamellae and by the formation of slip lines across unfavourably oriented pearlite colonies. Bleakney (4) from tensile tests on a 0.5 C steel concluded from the appearence of cracks across the pearlite colonies that final fracture was nucleated there.

As a result of microscopic examination of tensile and impact specimens, Burns and Pickering (5) suggested that nucleation of cleavage cracks in ferrite was relatively difficult but propagation easy whereas in the pearlite, nucleation was easy but propagation difficult.

Work carried out at Glasgow has confirmed that the type of deformation damage produced depends on the stress state (6). Further work at Glasgow was concerned with severe tensile stress states and tests were carried out on small notched tensile specimens (7). It was found that very few defects were produced before the specimens fractured. The object of this work was to extend these investigations into the effects of severe tensile stress states. These tensile stress states were obtained in notched bend tests, the specimens being made sufficiently large so that the conditions were approximately plane strain in the centre of the specimens at the notch root. An advantage of notch bend tests is that

the stress conditions at the ends of the notch approximate to plane stress and are not as severe as at the centre so that final fracture is retarded by deformation taking place at the ends of the notch rootand it is possible to examine cracking at the centre before final failure. Plane bend, tensile and torsion tests were also carried out to compare the deformation under severe conditions with that under less severe. Curves have been drawn to show the variation in ductility with severity of stress state and an attempt was made to assess the defect distribution semi-quantitatively and relate this to the stress state. Examination of fractures was carried out and it was found that the process of fracture tended to cause opening out of the defects.

Medium carbon steels have the advantage that for this type of work, the strain induced damage is easily visible using optical microscopy. A disadvantage is that the pearlite, having a lamellar structure, is inhomogeneous and anisotropic so that the stress fields are not uniform and may vary from grain to grain. For the purposes of this work, it has been assumed,however, that the stress fields are uniform or vary as if the material were isotropic. Taken over a number of grains, this assumption should not introduce too great an

error, the average grain diameter being approximately 0.001 m.m.

Chapter 2

PARAMETERS OF THE STRESS STATE

2.1 Definitions

The stress parameters to be used are the mean stress and effective stress defined as:-

$$\text{Mean stress} \quad \sigma_m = \frac{\sigma_1 + \sigma_2 + \sigma_3}{3}$$

$$\text{Effective stress} \quad \bar{\sigma} = \sqrt{\tfrac{1}{2}\left[(\sigma_1 - \sigma_2)^2 + (\sigma_2 - \sigma_3)^2 + (\sigma_3 - \sigma_1)^2\right]}$$

σ_1, σ_2, & σ_3 are the principal stresses and both the above quantities are invariants of the stress system.

The mean stress is the average of the principal stresses and can be thought of as the mean of the stresses acting normally to planes of principal shear stress. It may be expected that as damage accumulates on the shear planes during deformation, the normal stresses, if tensile will tend to promote opening of defects. The mean stress should thus influence the fracture behaviour.

The effective stress is proportional to the root mean square of the principal shear stresses and may be thought of as a statistical measure of the intensity of the shear stresses which governs the deformation of the metal.

The measure of strain which has been found to describe

the effective plastic strain in the material is defined by:-

$$\bar{\varepsilon}_p = \int \sqrt{\frac{2}{9}\left[(d\varepsilon_1^p - d\varepsilon_2^p)^2 + (d\varepsilon_2^p - d\varepsilon_3^p)^2 + (d\varepsilon_3^p - d\varepsilon_1^p)^2 \right]}$$

where $d\varepsilon_1^p$, $d\varepsilon_2^p$, $d\varepsilon_3^p$ are principal plastic strain increments. $\bar{\varepsilon}_p$ is a scalar quantity and is always taken to be positive.

The dilation component of the strain analagous to the mean stress is not considered as the volume change during plastic deformation is negligible.

In a tensile test, $d\varepsilon_2^p = d\varepsilon_3^p = -d\varepsilon_1^p / 2$

This gives $\bar{\varepsilon}_p = \int d\varepsilon_1^p$

$$= \log_e \frac{l_1}{l_0}$$

where l_1 and l_0 are the final and initial lengths of the specimen.

In torsion, $d\varepsilon_1^p = -d\varepsilon_3^p$

$$d\varepsilon_2^p = 0$$

$$\bar{\varepsilon}_p = \frac{2}{\sqrt{3}} \int d\varepsilon_1^p$$

The strain is normally measured as the angle of twist of the specimen θ .

The shear strain $\gamma = \tan \theta$

$$\bar{\varepsilon}_p = \frac{\gamma}{\sqrt{3}}$$

2.2. Constraint Factor

A quantity of interest in describing the stress state is its so called degree of triaxiality, a fully triaxial state being one in which the principal stresses are equal and have the same sign so that the values of the shear stresses are zero and no plastic deformation can occur. As the principal stresses are varied, the conditions deviate from triaxiality and allow plastic flow, the amount possible depending on the degree of triaxiality and the fracture susceptibility of the material.

It has been suggested that the degree of triaxiality of a stress system could be represented by the quantity $\sigma_m / \bar{\sigma}$ see for example (8). It can be seen by substitution into the expressions for mean and effective stress that if the principal stresses are equal and tensile, the value of the ratio tends to infinity, whereas in the case of a pure shear stress i.e. $\sigma_1 = -\sigma_2$; $\sigma_3 = 0$, the value is 0.

A suitable name for the ratio $\sigma_m / \bar{\sigma}$ would be the constraint factor since systems of high triaxiality are usually produced in regions of material which are constrained from deforming by surrounding material under different stress states.

For the tests carried out during this investigation, the constraint factors were found as follows:-

In torsion $\sigma_2 = -\sigma_1$; $\sigma_3 = 0$

Thus $\sigma_m = 0$

In the tensile test before plastic instability and in the plane bend test at the outside surface, only one principal stress is acting and substitution gives a value of 1/3 for the constraint factor. When necking takes place in the tensile test, there is a concentration of stress and the stress state becomes slightly more severe. The constraint factor can be found using the Bridgmann correction factor (9) as in appendix 1. In the plane bend test, a transverse compressive stress builds up towards the neutral axis so the constraint factor becomes less below the outer surface of the bend.

In the notch bend test, the constraint factor at the surface of the notch root was used as fracture was seen to start there. In the centre of the root, for a specimen of sufficient width, the conditions approximate to those of plane strain; the stresses acting are are σ_1 along the bar and σ_2 along the notch, σ_3 normal to the notch surface being zero as a boundary condition.

At the root of the notch, σ_2 can be written as equal to α

$\alpha\,\sigma_1$ if the strain along the notch root is zero. α varies from approximately 0.3 for elastic conditions to 0.5 when plastic flow is fully developed.

The mean stress is $\dfrac{\sigma_1 + \sigma_2}{3}$

$$= \frac{\sigma_1}{3}(1 + \alpha)$$

The effective stress is $\sqrt{\tfrac{1}{2}(\sigma_1 - \sigma_2)^2 + \sigma_2^2 + \sigma_1^2}$

$$= \sigma_1\sqrt{1 - \alpha + \alpha^2}$$

$$\frac{\sigma_m}{\bar{\sigma}} = \left(\frac{1+\alpha}{3}\right)\frac{1}{\sqrt{1-\alpha+\alpha^2}}$$

For $\alpha = 0.3$ $\quad \sigma_m/\bar{\sigma} = 0.49$

For $\alpha = 0.5$ $\quad \sigma_m/\bar{\sigma} = 0.58$

2.3. Stress Field for a Notched Bar

Fig. 1 shows the variation of the constraint factor below the notch root for the case of a hyperbolic notch under biaxial loading and plane strain conditions. The material is elastic and $\alpha = 0.3$ (10). The conditions are not strictly the same as for the Charpy notch in an elastic - plastic material but there are no suitable solutions available as yet for this case. Fig.1, however, gives an indication of

the stress variation that will occur. The constraint factor is seen to increase rapidly just below the root, the conditions at the surface being less severe.

Chapter 3

EXPERIMENTAL METHOD

3.1. Materials and Treatment

The material used for most of the tests was an E.N.8 plain carbon steel which contained about 0.4 to 0.5% of carbon giving a microstructure with just over 50% pearlite. The material was received in one inch square sections and was cut into lengths of 1 ft. prior to heat treatment.

Heat treatment consisted of heating to 900 deg.C for three hours followed by furnace cooling to room temp. This gave a fairly coarse pearlite with mixed interlamellar spacing. The bars were then machined into test pieces for notch bend, plane bend tensile and torsion tests.

The notch bend test pieces were 1ft. long with a 1in. square section and were machined by surface grinding to remove scale and the small decarburised layer left by heat treatment. A standard Charpy cutter was used to machine a 0.25in. deep notch in the centres of one surface of the bars, the notch having a 0.2m.m. root radius.

For the plane bend tests the specimens were 1ft. long and after being surface ground were milled to 1 in. by 0.75ins. cross section.

The tensile test pieces were 0.35 ins. diameter with a parallel length of 2 ins.. The ends were 0.5 ins. diameter and screw cut. A fillet radius was cut between the ends and the parallel portion.

The torsion test pieces were 0.5 ins. diameter with a 2.5 ins. parallel length, the ends being cut to fit the testing machine.

For comparison purposes, some tests were also carried out on a plain carbon steel containing about 0.6% carbon with a structure composed of approximately 75% of pearlite. The steel was heat treated before machining by heating to 850 deg. C for three hours followed by furnace cooling.

3.2. Mechanical Testing

The mechanical testing with the exception of the torsion tests was carried out on an Instron TT (M) machine calibrated in metric units and of 5,000 kg. capacity. The torsion testing was carried out on an Avery machine of 15,000 in.lbs. capacity.

The rig used for the notch bend tests is shown schematically in fig.2. Four point bending was used and the rate of deflection of the centre of the specimens was 0.05 cms. per minute, load - deflection curves being plotted

by the recorder on the machine. 10 specimens were tested, A1 to A7 were strained by different amounts up to the maximum load, A8 & A9 to between the maximum load and fracture and A 10 to fracture.

The plane bend tests were carried out using three point loading as four point loading produced loads and deformations outside the capacity of the machine and test rig. Furthermore, to fracture the E.N.8 bar, it had to be strained as far as possible in three point bending and further bent by placing it on end in the machine and compressing the two ends. Bars of the 0.6 C steel could be strained to fracture in three point bending.

Four tensile specimens of E.N.8 steel were tested, one to fracture, one to the U.T.S. and the other two to strains between the U.T.S. and fracture. Load extension curves were obtained using a strain gauge extensometer on a gauge length of 1 inch.

Torsion tests were carried out on both steels and as there was no recorder on the machine, load and angle measurements over the whole specimen length were made at intervals of time.

3.3. Estimation of Strains

3.3. Estimation of Strains The strains in the notch tests were estimated using the analysis in appendix 2 (11).

In the plane bend tests, gauge marks approximately $\frac{1}{4}$ inch apart were inscribed on the outer surface where the deformation was approximately constant and were cut so that the longitudinal and transverse strains could be measured. Measurement of the displacement of these marks was carried out at low magnification on a Vickers projection microscope using the calibrated micrometer screws on the specimen stage.

In the case of the specimens strained to fracture, the breaks occurred between the gauge marks so the above method could not be used. The strains in these specimens (and others to serve as a check on the method) were found using values of the radius of curvature of the outer surface and the depth of the neutral axis. An estimation of the depth of the neutral axis could be made by examination of the ground surface of the bar, this appearing duller where the deformation was fairly severe but leaving a bright band near the centre. The position of the neutral axis was taken to be at the centre of the brighter band, this being about

1.4 cms. from the outer surface in a fractured E.N.8 specimen. The measurement of curvature was made on the projection microscope by finding the length of a chord on the outside of the bend and measuring the length of the line from the centre of the arc to the centre of the chord, these distances being foud with the aid of lines ruled on the viewing screen of the microscope.

Strains at different depths from the outer surface of the plane bend specimens could be found from the strain at the outer surface and the depth of the neutral axis using the assumptions that plane sections of the bars remained plane after bending and that the strain at the neutral axis was zero.

In the tensile tests taken into the necking region, the strains at different parts of the neck were measured from the diameters, the axial strain across a particular section of the specimen being assumed uniform.

In both the tensile and plane bend tests, the strains were expressed logarithmically.

In the torsion test, shear strains were measured from tan (angle of twist). The angles of twist were measured from the angle of rotation of the specimen and from the

angle of the microstructure.

3.4. Microscopical Examination

All specimens were sectioned and prepared for microscopical examination. In the case of the notch bars sections were cut from the centre perpendicular to the notch so that the plane strain regions could be examined. In the plane bend and tensile specimens the sections were cut from the centres of the bars in the directions of the principal strains. In the torsion test, the region of maximum strain was at the surface so they were prepared by polishing a small amount from the surface.

Etching of all samples was carried out in a 4% solution of nitric acid in ethanol and examination and photography carried out using a Vickers projection microscope. In all the photographs, the horizontal directions lie along the longitudinal axes of the specimens.

3.5. Defect Counting.

There are two types of strain induced defect that occur in pearlite, these being of the slip line type as in fig. 3 and the slip band type, fig. 4. The latter occur mostly in compressive stress states although some are seen in torsion. As tensile stress states are being considered the slip band

has been ignored for counting purposes.

The severity of the slip line type of defect varies and although there is no definite distinction, it is convenient to classify them into two categories, major defects as in fig. 3 which traverse a pearlite colony completely and follow straight paths and minor defects which do not traverse the whole grain and which often follow irregular paths across the lamellae.

No defects of the major variety were observed in samples of the undeformed steel but a number of minor defects was present. As the material was strained, the number of minor defects increased showing that some of them were strain induced as were the major defects. Slip lines similar in appearance to the minor defects have been observed during the growth of lamellar lithium flouride - sodium flouride eutectics when the nuclei are made to grow in unfavourable directions, rotation of the lamellae towards more favourable orientations resulting in the formation of short slip lines (12).

To allow for the growth defects, counts were carried out on undeformed material which yielded values of about 5 to 6 defects per 0.01 sq. m.m.. In this work, a figure of 8 defects per 0.01 sq. m.m. has been taken as representing

plastic flow to have occurred in the material. The value has been chosen rather high so as to be definitely in the region of plastic deformation.

As with other quantitative metallographic techniques, the defect counting cannot be claimed to be accurate but it is hoped that sufficiently consistent results have been obtained so as to give a picture of the relative distribution of the defects.

Defect counting was carried out on the Vickers projection microscope at a magnification of 2,000 times using an oil immersion lens, the illumination being provided by a mercury vapour lamp and a green filter. The specimen stage was fitted with micrometer screws and was clamped so that the stage could be moved in the direction of and at right angles to, the ground glass viewing screen. The specimens were clamped on the stage so that the longitudinal axes lay along the directions of stage motion.

Counts of the total number of defects, i.e. major + minor were made over 0.01 sq. m.m. areas. At the magnification used, the width of the viewing screen represented a distance on the specimen of 0.08 m.m. and the distance the field of

view was traversed for each count was 0.125 m.m. making an area of 0.01 sq. m.m.. A line was inscribed across the viewing screen and the number of defects crossing this line over the width of the screen as the field of view was traversed 0.125 m.m. was recorded for each count. Counting proceeded as the field of view was traversed so a first impression count was made. This had the advantage that only the more obvious defects were noticed which probably eliminated a large number of growth defects.

For some specimens, estimates of the number of major defects alone were made, the results being expressed as number per sq. m.m. as there were far fewer. The area over which the number was counted was larger, the length of the traverse being several millimetres and depending on the size of the specimen.

3.6. Effect of Strain Rate

The deformation behaviour of a material is known to depend on the strain rate and in this investigation using different types of test and specimen, the strain rates have not been constant. It has been found, however, that for this material in the range of strain rates used, there is little

variation in properties (13). To confirm this, four notch bend tests were carried out on 0.60 steel samples at strain rates differing by a factor of twenty and fairly similar load - deflection curves were given. ~~(Figure 6)~~

3.7. Strain Field below Notch

Work done on the deformation of mild steel has shown that the strained area can be etched using Fry's reagent (e.g. 14). After straining, the steel is heated to 300 deg. C at which temperature, carbides are precipitated in the strained areas which are subsequently darkened on etching. An attempt was made to outline the strained area beneath the notch in bent samples but the amount of pearlite was too great for any preferential etching of the strained region to be visible.

Micro - hardness tests were also carried out on the notched specimens to try and find the deformed region but the scatter was too great for the results to have any meaning.

Chapter 4

EXPERIMENTAL RESULTS

4.1. Notch Bend Tests

Fig. 5 shows the load - deflection curves for both the E.N.8 and 0.6C steels up to the fracture points. The elastic ranges are comparable but the 0.6C steel shows a greater work hardening rate and does not show a maximum in the curve.

Fig. 6 is a bending moment - deflection curve for the E.N.8 steel and is an average curve plotted from the points to which the ten specimens were tested.

Microscopical examination that cracking in the notch root first occurred in specimen A 4 and appeared to be initiated on the surface of the root (fig. 7). The strain in the root for specimen A4 was taken as the strain to fracture for the notched E.N.8 steel. The calculation of this strain was made using the analysis of appendix 2 which assumes linear elastic behaviour, this solution having to be used as there is no elastic - plastic solution available. This approximation should not be expected to involve a great error as the rate of work hardening of the material as shown by the tensile curves is fairly high. Fig. 6 was used

for the strain calculation and the construction lines are shown dotted.

From A4 until the maximum load was reached, the crack length increased, spreading from the surface. The initial crack was fairly wide and was intergranular. In A8 and A9 finer cracks could be seen continuing from the initial crack which for the most part followed the ferrite - pearlite boundaries. Fig. 9 shows a network of fine cracks in the ferrite pearlite boundaries and fig. 8 shows a crack following ferrite boundaries and inclusions. Rapid failure then occurs and the fracture is trans - granular.

The defects below the notch were of the slip line type, by far the majority being minor slip lines, a few major defects such as those in fig. 3 from specimen A9, being seen in specimens subsequent to A6. Tables 1 & 2 show defect counts from specimens A4 & A7 respectively from points below the notch as shown.

4.2. Plane Bend Test

Table 3 shows the degree of straining in each of four specimens tested, B1 being the fractured bar. Table 4 shows a series of measurements of the longitudinal and transverse strains made on B3 to check that the stress

state on the outer surface of the bar during plastic deformation was approximately uniaxial. Exam If the stress was uniaxial, the transverse strain would be half the longitudinal, there being no volume change during plastic deformation. From the table this can be seen to be approx. true, the discrepancy for smaller strains likely to be due to errors in displacement measurement.

The grain shape was much altered by deformation, being elongated in the direction of stress application in the tensile side and deformed at right angles to this in compression. In tension, the defects were of the slip line type, the majority being of the minor type but with an appreciable number of major defects in the more highly strained material. In compression, the defects were of both slip line and slip band type.

The results of defect counting in the four bars are shown in fig. 10, from which it appears that most of the defect formation occurred over a relatively small strain range after which the increase in number became slower. A count of major defects is shown in table 5 and this too shows signs of a saturation value being reached but at a

higher value of the strain. The count for specimen D1 also includes the cracking referred to in the following paragraph.

A feature of the structure in the fractured specimen was the large number of cracks in the pearlite alongside the fracture surface. Fig. 11 is a photograph of these cracks in an unetched specimen and it is seen that many of them appear to be wider in the centre than at their ends. The angle of the cracks appears to be mainly at 45 deg. to the direction of strain. Fig. 12 shows that cracking occurs along major slip lines. Normally the cracks did not extend beyond the pearlite colony in which they were formed.

4.3. Tensile Test

Fig. 13 shows the load - extension curves to fracture for the E.N.8 and 0.60 steels. Table 6 shows the amount to which the four E.N.8 tensile specimens were strained together with the constraint factors found as in appendix 1. T1 is the specimen strained to fracture.

Defect counts from these specimens are shown in table 7 and, as can be seen, saturation values seem to have been reached in all cases. As with the plane bend test, four counts have been made at each strain and averaged. To try and estimate strains at which defects are first formed, a tapered

tensile specimen was tested and the variation in the number of defects with strain plotted in fig. 14.

4.4. Torsion Test

Fig. 15 shows the torque - twist diagram for the E.N.8 torsion test to failure, the angle of twist being measured over the specimen length. Table 8 shows values of the strain measured from the angle of twist and the micro - structure, these values being comparable. From fig. 16 of the fracture of the specimen, it is seen that the strain is locally higher at the fracture surface and this strain measured from the angle of the micro - structure has been taken as the strain to fracture.

The defects were counted on a section cut obliquely to the surface of the bar so defects at different strains could be counted. The results are in fig. 17.

Chapter 5

DISCUSSION

Fig. 18 shows the constraint factor $\sigma_m/\bar{\sigma}$, plotted against the strain to fracture for both E.N.8 and 0.60 steels and demonstrates a marked decrease in ductility with increasing severity of stress state, the lower carbon steel showing the greater ductility as expected. The effect of constraint factor on ductility could also be seen by examination of the notched bars bent to near fracture. Cracks were seen in the centres of the bars at the base of the notch root where the conditions approximated to plane strain, these cracks being absent near the ends of the notch where the conditions were not so severe, plastic deformation in the form of dimpling occurring instead.

Counts of the total number of defects, major + minor, indicate that in the plane bend, tension and torsion tests, a saturation in thenumber occurs, the saturation value in the tensile and plane bend tests being greater than in torsion partly due to some of the deformation in the latter occurring as wide slip bands as well as slip lines. In the notch bend test, it is difficult to determine whether saturation is

reached, table 2 from specimen A7 indicating that it may have been as values of the defect number are similar to those from the plane bend and tensile tests. It seems that most of the defects are formed at a low strain and it is possible that further deformation involves the growth of existing slip lines. Although the number of major defects continues to increase with the strain, there are indications in table 5 that these too may reach a saturation value.

It is probable that the principal mode of deformation is by slip parallel to the cementite lamellae and slip lines are only seen in grains that are unfavourably oriented with respect to the directions of maximum shear strain and which are unable to rotate to more favourable directions. The slip lines lie near to the directions of maximum shear strain i.e. at about 45 deg. to the principal stresses. In most cases, the slip lines make an angle of 45 deg. or more with the directions of the cementite lamellae. In most of the test pieces there were maximum shear strain directions at 90 deg. to one another so that the maximum mis - orientation of the lamellae is 45 deg.. Slip lines occurring at angles greater than 45 deg. e.g. those in fig.

3 and having lamellae parallel to one direction of maximum shear stress, yet slipping on another, are probably due to local constraint in the surrounding material preventing slip parallel to the lamellae.

Fig. 19 shows a plot of the constraint factor against strain at the onset of defect formation, this being taken as 8 defects per 0.01 sq. mm.. This strain depends to an extent on the stress state but not nearly to as great a degree as the strain to fracture. A point was obtained on the curve for each of the plane bend specimens due to the reduction in constraint factor with distance from the outer surface of each bar as a compressive stress builds up towards the neutral axis.

Although the stress state becomes more severe below the notch as indicated in fig. 1, fracture appears to start from the notch surface, fig. 7. This is due to the strain below the notch being insufficient to cause fracture even at the severer stress states. The strain falls off very rapidly below the notch, becoming about $\frac{1}{4}$ of its surface value at a depth below the notch of approx. the root radius. The error involved in calculating the strain in the notch root at fracture may be fairly high due to the approximations

used but a factor of 5 only brings the strain to 0.1 and makes little difference to fig. 18.

In the plane bend and tensile tests there was no indication in the form of surface cracks etc., that fracture was about to take place. In the plane bend test, failure would have occurred first at the surface where the strain and constraint factor were greatest. In the tensile test, failure was probably initiated in the centre of the bar as has been observed previously, e.g. (15), where the constraint factor is a maximum but the effective strain slightly less than at the surface.

In the torsion test, fracture was initiated at the surface and alongside the main fracture, there were a large number of smaller cracks as in fig. 20, the cracks having originated from machine marks in the specimen. The cracks appeared to be associated with regions of high deformation as in fig. 21 and this suggests that failure is due to the formation of regions of local instability. The cracks in torsion seemed to follow lines of major defects across pearlite colonies and it is probable that the defects have played a large part in the nucleation and propagation of cracks.

Examination of major defects such as in fig. 3 shows that the lamellae of ferrite and cementite are continuous across most of the defect lines but in some of them, especially in more highly strained specimens, some of the cementite lamellae appear to have been broken and these would provide a good crack nucleus. Only in the torsion test could cracks be seen forming on major defects but it is probable that fracture initiation in the other tests occurred in a similar manner. In the plane bend and tensile tests, the fractures were wholly transgranular and cracking probably followed major defect lines across the pearlite as these were plentiful.

Fracture of the notched bars was rather different partly because the number of major defects was less than in the other tests. Due to the higher mean stress, it would be expected that once a major defect is formed, it would be more likely to propagate, thus accounting for the small number present before final fracture occurs. Although cracking may start from the major defects, there are insufficient for the cracking to follow defect lines so the initial stable crack tends to follow the ferrite - pearlite boundaries as in figs. 8 & 9, these boundaries being weaker or subjected to higher local constraints than

the rest of the material.

When the crack becomes unstable in the notch bend test, its nature appears to change, becoming transgranular as in fig. 22 which also shows some subsidiary pearlite cracking. In one of the 0.60 steel specimens the unstable fracture was arrested before traversing the specimen due probably to the shear lip on the surfaces restraining motion of the crack in the centre (the crack had travelled further in the centre than at the edges). Examination of the crack tip at the centre of the bar showed that cracks across the pearlite lamellae preceded the main fracture(figs. 23 & 24. Most of these cracks were across the lamellae at angles of 45 deg. or more with the lamellar direction. The material through which the crack was propagating at this stage had been previously deformed only to a slight extent and there were no major defects in the surrounding pearlite.

The cracks seen in the E.N.8 plane bend and tensile tests appeared to be due to splitting open of major defects near the fracture surface and fig. 25 from the plane bend test shows that the distribution of the cracks follows a similar pattern to the distribution of major defects. Cracks such as these were only seen in the fractured specimens

and none were observed in specimens strained to near fracture. Table 3 shows that specimen B4 was strained to 0.52, yet from fig. 25 for specimen B1, there were about 70 cracks per sq. mm. at this strain and none in B4. Similarly no cracking was seen in B2 or B3 although these too were strained to where cracking was seen in B1. This effect was also present in the tensile tests and from table 6 and fig. 26 it can be seen that wide cracks were present in the fractured specimen T1 in parts of the neck that were strained the same amount as specimen T4 which showed no cracking. This cracking seems to occur at fracture and could be due to the passage of stress waves through the material. Cracking of this type is not seen in the torsion or notch - bend tests. In the former case this is probably due to the much less sudden energy release at fracture and in the latter case to the relatively low number of major slip lines. The cracks observed in the 0.60 notch bend specimen ahead of the main crack and described previously are similar in appearance to these, the main difference being that the former occur in material that has had very little prior plastic deformation but both could be due to a similar cause. The reason for the

pearlite failing first could be due to it being more susceptible than ferrite to the high strain rate any stress wave would have as it is more brittle. In the notch bend test, this effect could lead to the transition from intergranular to transgranular failure as the crack accelerates.

Chapter 6

CONCLUSIONS

The ductility of the materials tested has been shown to depend to a large extent on the degree of triaxiality of the stress state which has been represented by the ratio of the mean to effective stress.

The deformation of ferrite-pearlite structures is accompanied by the formation of slip line defects across the pearlite lamellae and when deformation is severe, some cracking occurs which can act as a nucleus for fracture initiation. The number of major defects required to promote failure is very much less when the stress state is severe and demonstrates the effect of a high mean stress in causing defects to open and propagate. Under less severe stress states, the number of defects appears to reach a saturation value after a certain amount of strain.

Where there are a large number of defects, the final fracture seems to be transgranular, but in the notched tests where the defects are few, the crack in its initial stages is intergranular becoming transgranular as its speed increases. An unstable crack seems to propagate by nucleating smaller cracks ahead of it, these cracks being for the most part

across the pearlite lamellae.

Defects in the highly strained pearlite near the fracture surfaces in the tensile and plane bend tests appear to have been opened up when final fracture occurred, indicating some effect due to stress waves at fracture.

Chapter 7

SUGGESTIONS FOR FURTHER WORK

1. It may be of practical use to compare the ductilities of different materials on the basis of curves of constraint factor against strain to failure. Such curves could be used to indicate the relative notch sensitivity of the materials.
2. The work could be extended to include other factors influencing ductility such as the strain rate and temperature and the inter-relation of each.
3. To form a complete picture of deformation and fracture mechanisms in carbon steels, the damage to the ferrite phase should be investigated, which would involve electron microscope work to evaluate dislocation configurations etc.
4. Further work is required on the mechanism of fracture propagation in pearlite and to investigate the similarities and differences between the damage produced ahead of a moving crack in previously undeformed material and the pearlite cracks alongside the fracture in heavily deformed grains.

REFERENCES

1. P. Jenkins et al. J. Iron & Steel Inst. 1942 No. 1 p 51
2. J.C. Danko & R.D. Stout. Supp. Welding J. 1955 March
3. K.E. Puttick. J. Iron & Steel Inst. 1957 Feb. p 157
4. H.H. Bleakney Canadian Met. Quart. Vol.2 No.4 1963
5. K.W. Burns & F.B. Pickering. J. Iron & Steel Inst. 1964 Nov. p.899
6. T. Malcolm. Final Year Hons. Project Report, Glasgow Univ. 1966
7. S.P. Fitzpatrick " " " " " " " 1967
8. J.R. Rice & G.F. Rosengren. J. Mech. Phys. Solids Vol.6 1968 p.1
9. P.W. Bridgmann. "Studies in Large Plastic Flow & Fracture" 1964 Harvard Press.
10. "Stress Analysis for Fracture" Post-grad. course notes Univ. of Glasgow April 1968
11. J. Orr Private Communication
12. D.D. Double, P.Truelove & A. Hellawell. J. Cryst. Growth Vol. 2 1968
13. H.G. Baron J. Iron & Steel Inst. Vol.182 p.254 1956
14. J.F. Knott & A.H.Cottrell. J.Iron & Steel Inst. Vol. 201 p.249
15. K.E. Puttick Phil. Mag. 1959 Vol.4 p. 964

FIG. 1

$\frac{\sigma_m}{\bar{\sigma}}$ BELOW NOTCH ROOT

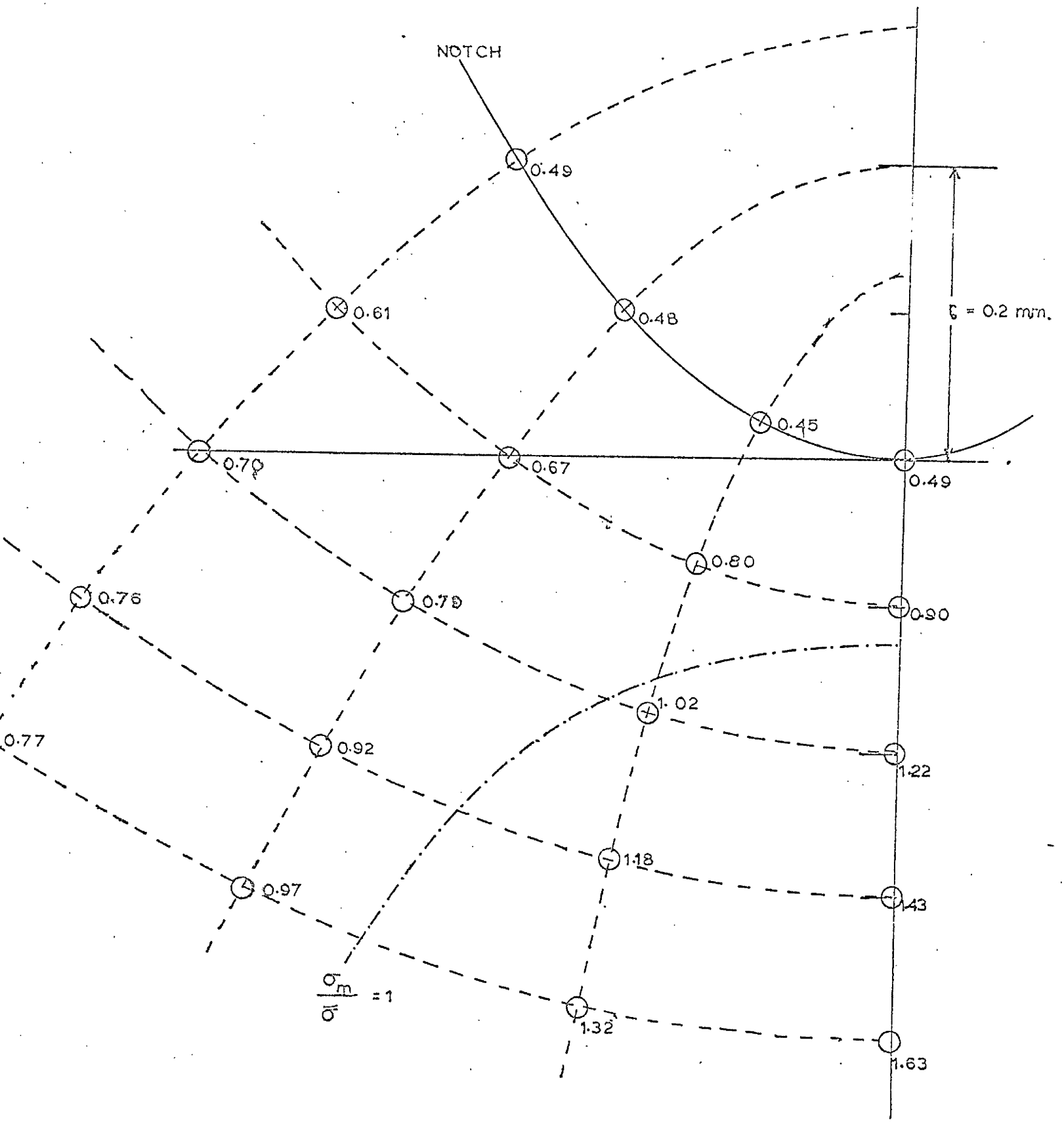

FIG 2

NOTCH BEND RIG

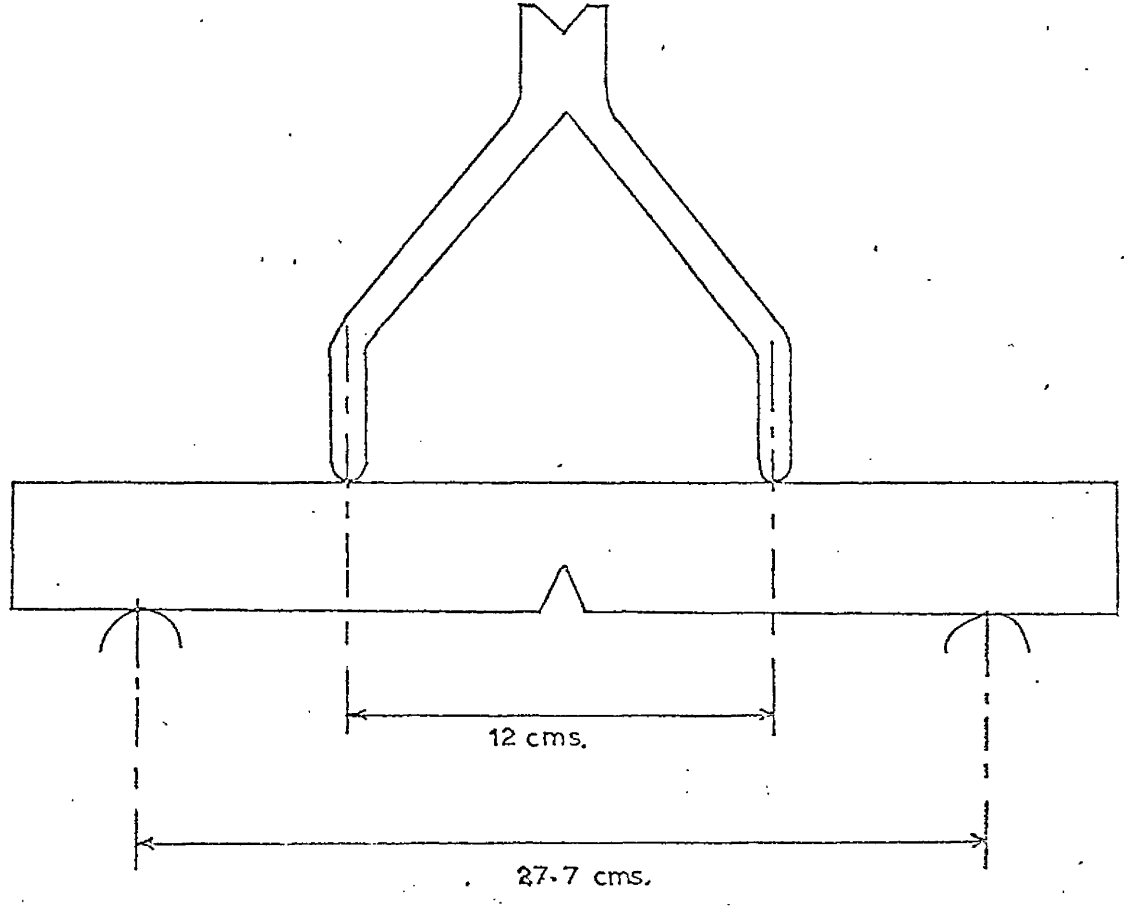

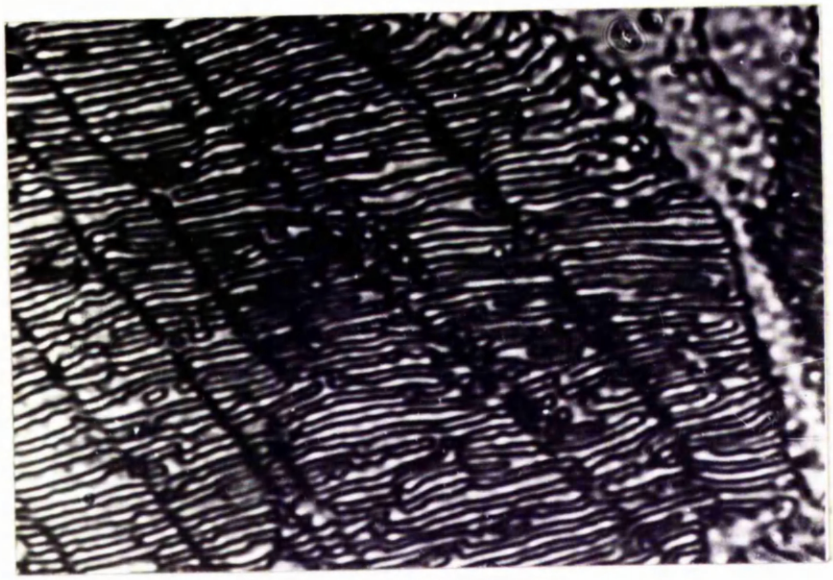

Fig. 3 X 3,500

Fig. 4 X 2,000

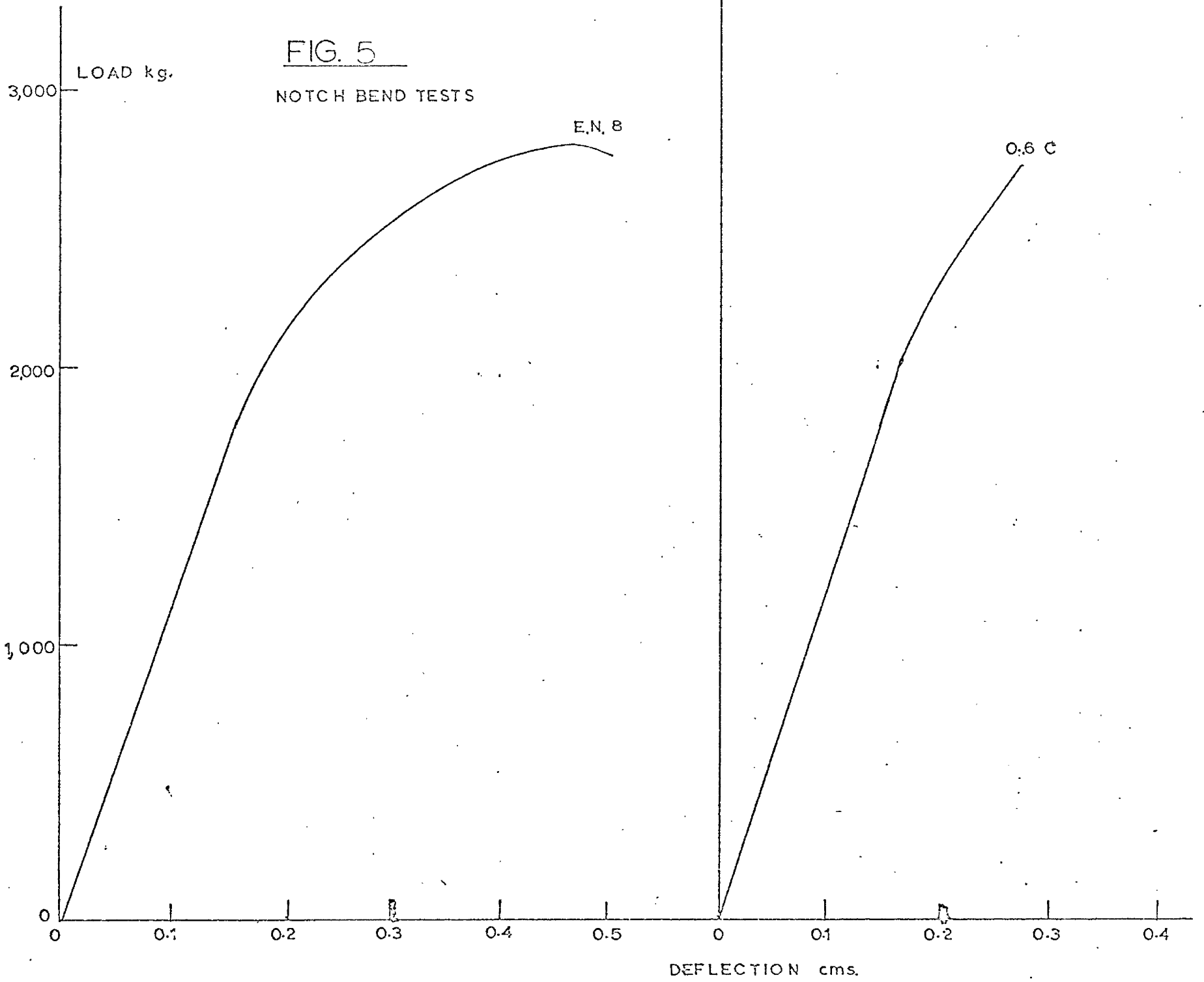
FIG. 5
NOTCH BEND TESTS
LOAD kg.
3,000
2,000
1,000
0
E.N. 8
0.6 C
0
0·1
0·2
0·3
0·4
0·5
0
0·1
0·2
0·3
0·4
DEFLECTION cms.

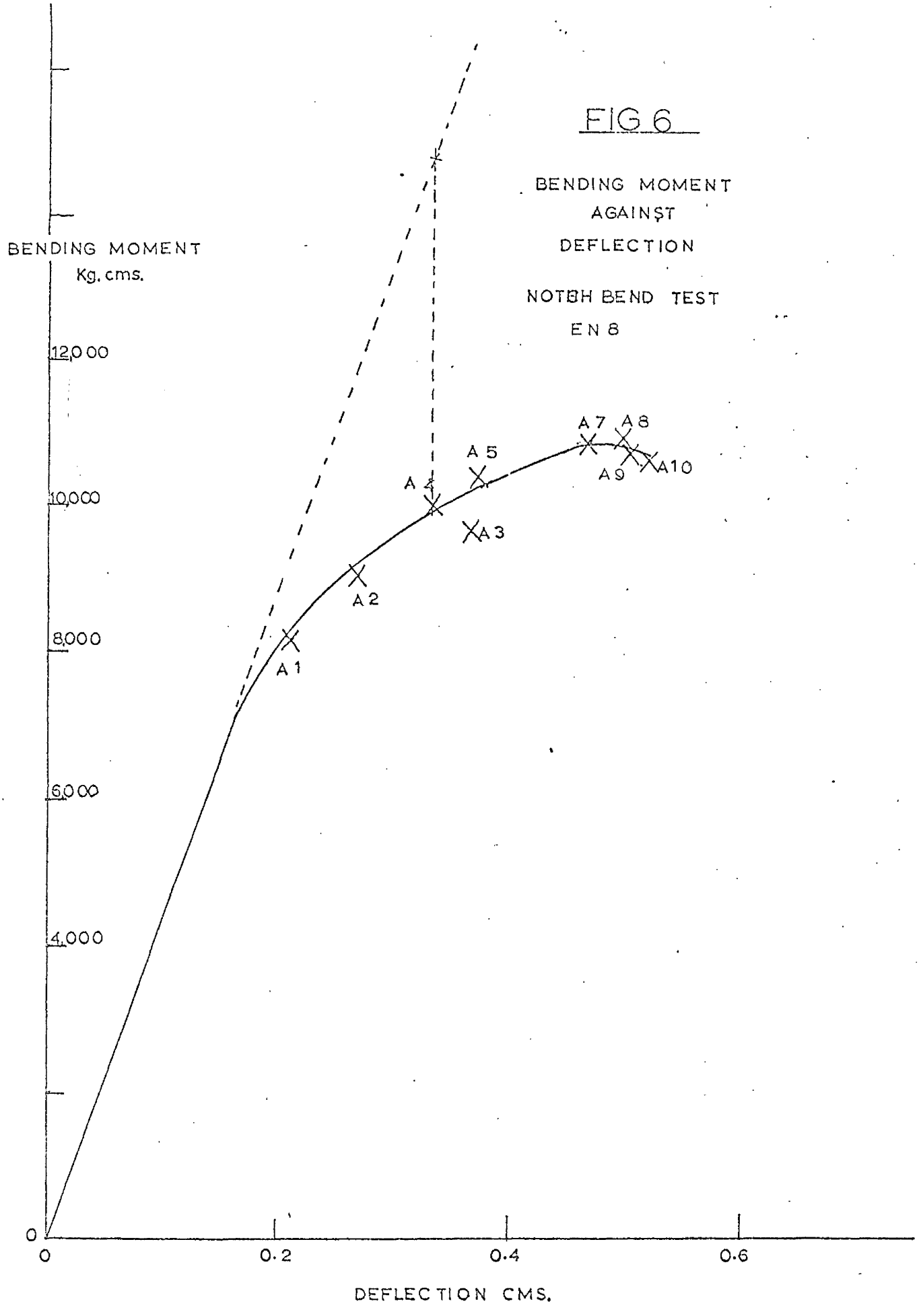
FIG 6
BENDING MOMENT AGAINST DEFLECTION
NOTCH BEND TEST
EN 8
BENDING MOMENT
Kg. cms.
12,000
10,000
8,000
6,000
4,000
0
0
0.2
0.4
0.6
DEFLECTION CMS.
A1
A2
A3
A4
A5
A7
A8
A9
A10

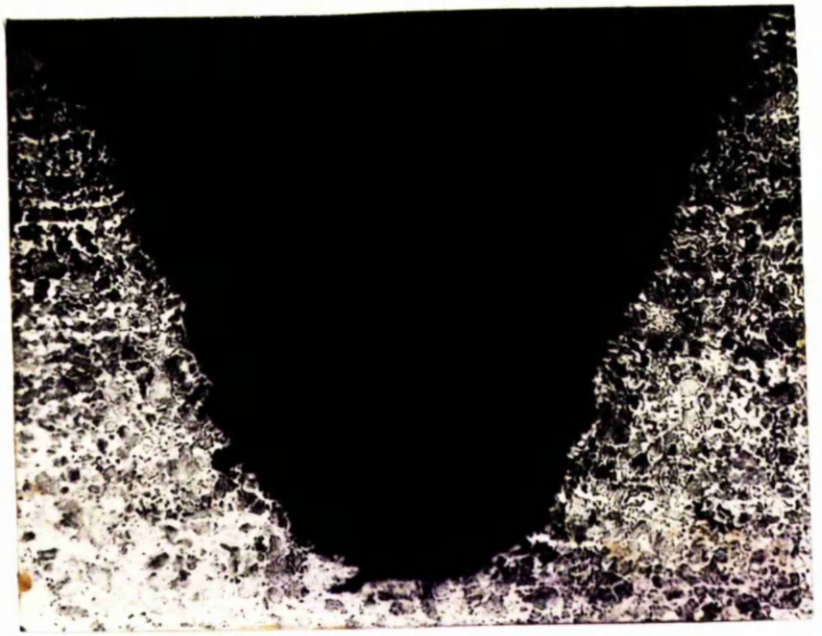

Fig. 7 X 70

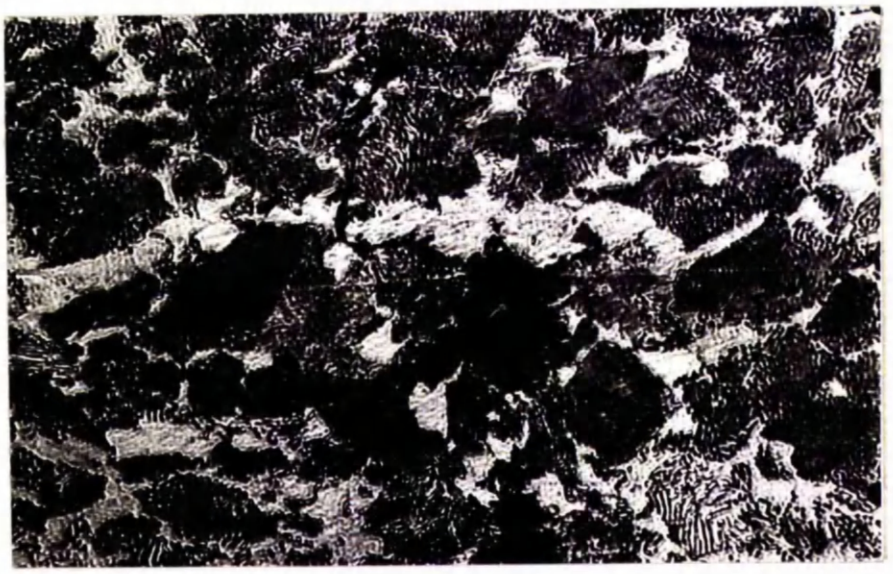

Fig. 8 X 500

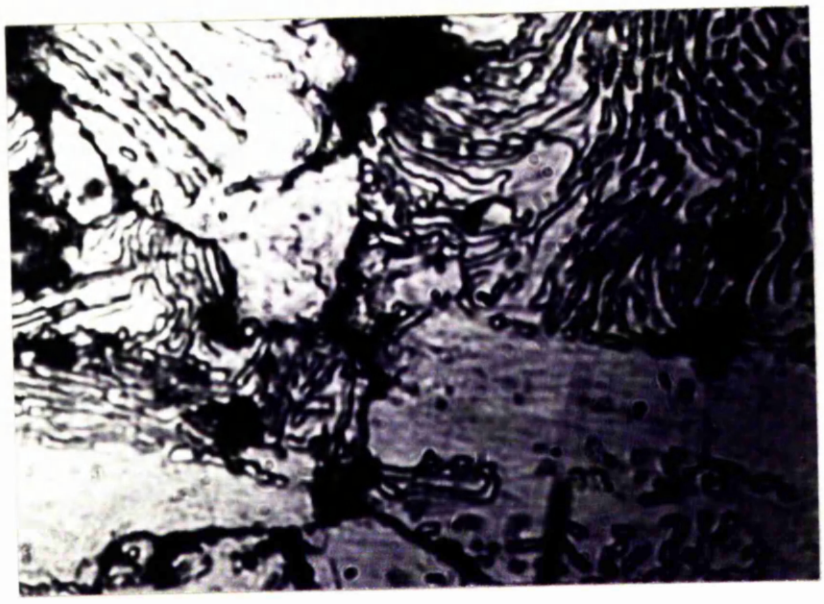

Fig. 9 X 3,500

Table 1

Defect Count below Notch Root Specimen A4

Distance below Notch Root 0.125mm units	Distance from Notch Root in 0.125 mm units (0 is position of centre of root)								
	4	3	2	1	0	1	2	3	4
1	4	8	8	8	8	8	7	8	5
2	6	7	4	10	9	12	6	7	6
3	4	5	8	9	7	7	9	8	5
4	5	6	4	6	5	8	6	5	4
5	4	5	3	9	9	2	5	6	4
6	3	4	5	4	5	7	7	8	5
7	5	5	4	5	7	7	4	6	4
8	5	6	6	7	4	3	5	4	4
9	7	3	5	6	6	3	4	4	1
10	4	4	5	6	5	6	3	4	3
11	2	4	4	3	1	4	4	5	5
12	3	3	4	6	2	6	3	4	4
13	5	5	7	3	5	2	2	4	4
14	4	2	4	3	5	3	5	3	4
15	2	4	4	1	5	3	3	5	3
16	2	3	4	2	5	4	4	4	4

(..... indicates approx. region where most deformation has occurred)

Table 2

Defect Count below Notch Root A 7

Distance below Notch Root 0.125 mm units	Distance from Notch Root in 0.125 mm units (0 is position of centre of root)													
	5	4	3	2	1	0	1	2	3	4	5	6	7	8
1	7	8	5	2	3	3	4	5	5	5	5	7	3	6
2.	8	5	7	10	14	13	8	7	9	6	12	5	5	4
3	4	13	9	11	5	10	9	10	9	11	5	5	4	5
4	8	6	10	4	10	8	13	9	7	10	12	7	6	6
5	10	10	9	9	15	11	5	8	9	6	6	9	2	6
6	7	14	8	8	9	11	12	4	11	7	7	9	9	3
7	6	9	7	6	9	9	4	8	8	11	6	7	10	5
8	12	7	5	5	7	8	9	6	8	9	3	5	5	2
9	8	6	7	5	5	8	8	8	5	6	8	6	7	2
10	6	7	3	5	9	5	9	4	8	9	5	7	7	4
11	5	5	7	4	10	5	3	3	5	4	6	6	6	7
12	3	4	8	5	4	8	5	3	3	6	4	5	5	3
13	6	5	6	6	4	4	5	9	4	3	5	2	9	6
14	2	6	3	5	6	4	3	4	3	5	9	5	8	6
15	4	9	6	4	3	4	6	5	7	4	9	3	3	4
16	4	7	5	7	6	3	4	6	3	6	5	1	3	4

Table 3

Plane Bend Test

Specimen	Outer radius of Bend cms.	Depth of Neutral axis from outside of bend cms.	Radius of Neutral Axis cms.
B 1	3.4	1.4	2.1
B 2	7.4	1.0	6.4
B 3	6.4	1.2	5.2
B 4	4.1	1.3	2.8

Specimen	Long. Strain from Gauge Marks	Long. Strain from radius
B 1	-	0.64
B 2	0.214	0.21
B 3	0.255	0.23
B 4	0.489	0.52

Table 4

Plane Bend Test

Test Piece B 3

Bending Moment Kg cm	Long. Strain	Trans. Strain
0	0	0
10,450	0.027	-
12,900	0.043	-
14,000	0.066	-
15,700	0.086	0.015
17,600	0.113	0.048
17,400	0.166	0.058
16,500	0.191	0.086
15,700	0.223	0.104
14,000	0.239	0.113
13,400	0.255	0.131

FIG. 10

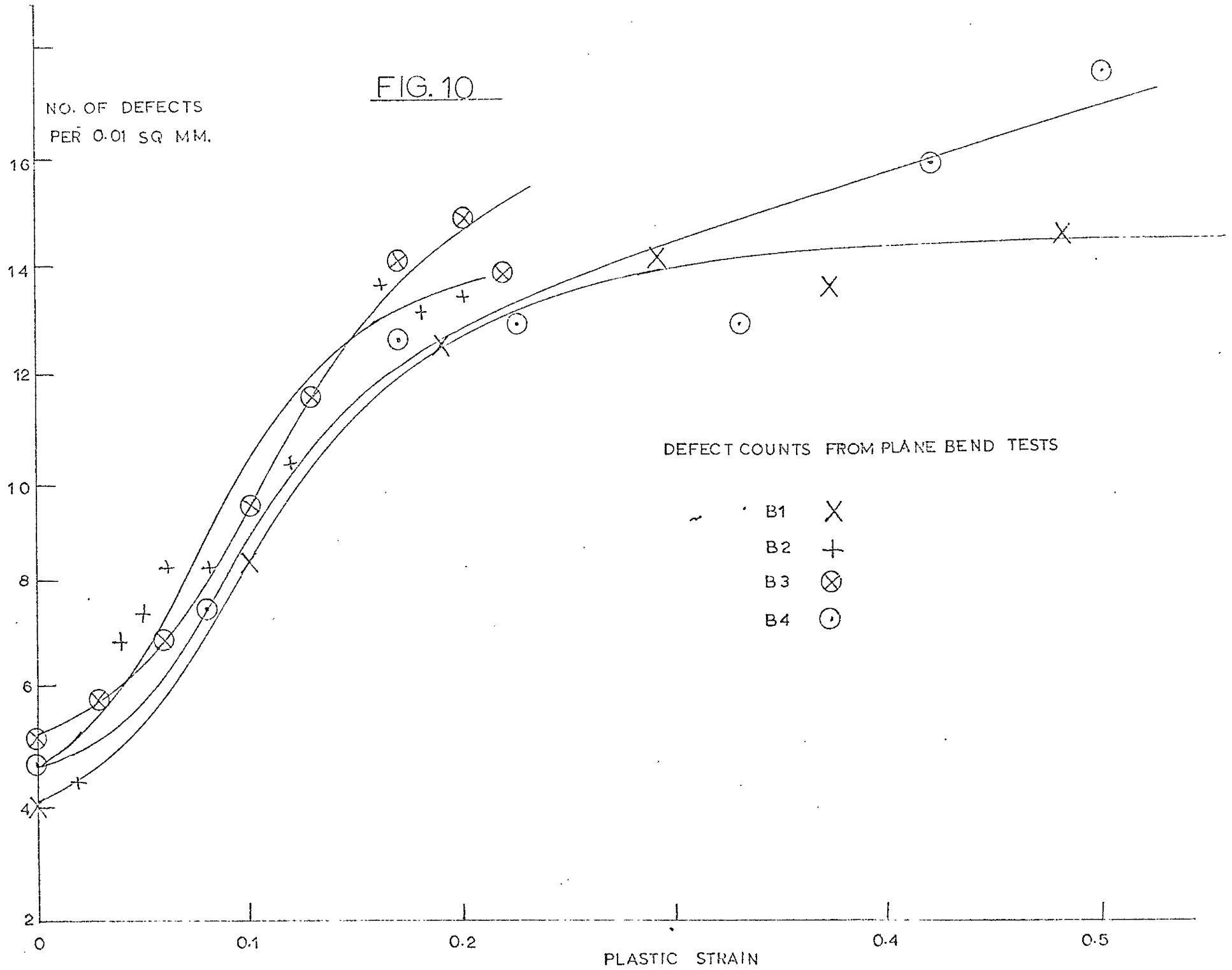
NO. OF DEFECTS
PER 0.01 SQ MM.
16
14
12
10
8
6
4
2
0
0.1
0.2
0.4
0.5
PLASTIC STRAIN
DEFECT COUNTS FROM PLANE BEND TESTS
B1
B2
B3
B4

Table 5

Plane Bend Test

Major Defects against Strain

	Strain	Defects /mm^2
Specimen B 1		
	0.64	214
	0.56	220
	0.49	250
	0.41	200
	0.33	163
	0.28	64
	0.23	10
	0.19	0
Specimen B 2		
	0.21	22
	0.20	0
Specimen B 3	0.23	10
	0.22	0
Specimen B 4		
	0.50	70
	0.44	89
	0.38	120
	0.26	85
	0.20	12
	0.19	0

Fig. 11 X 50

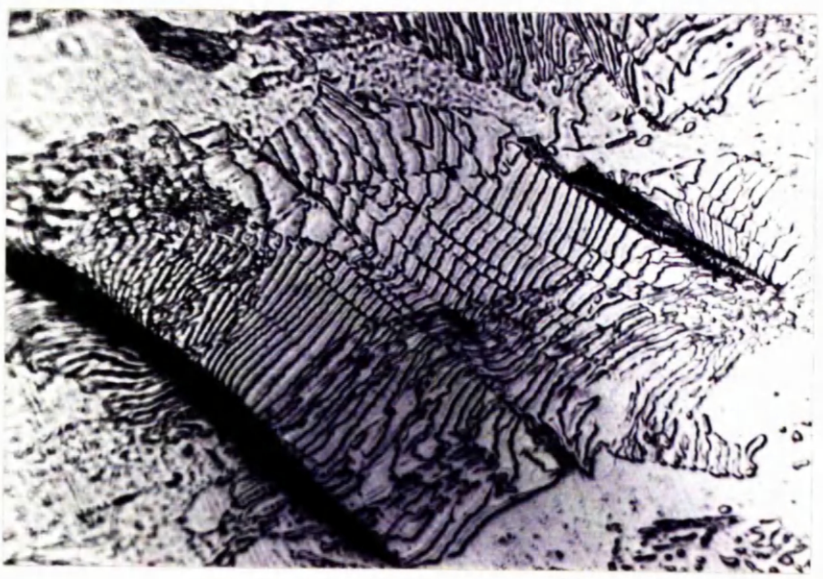

Fig. 12 X 2,000

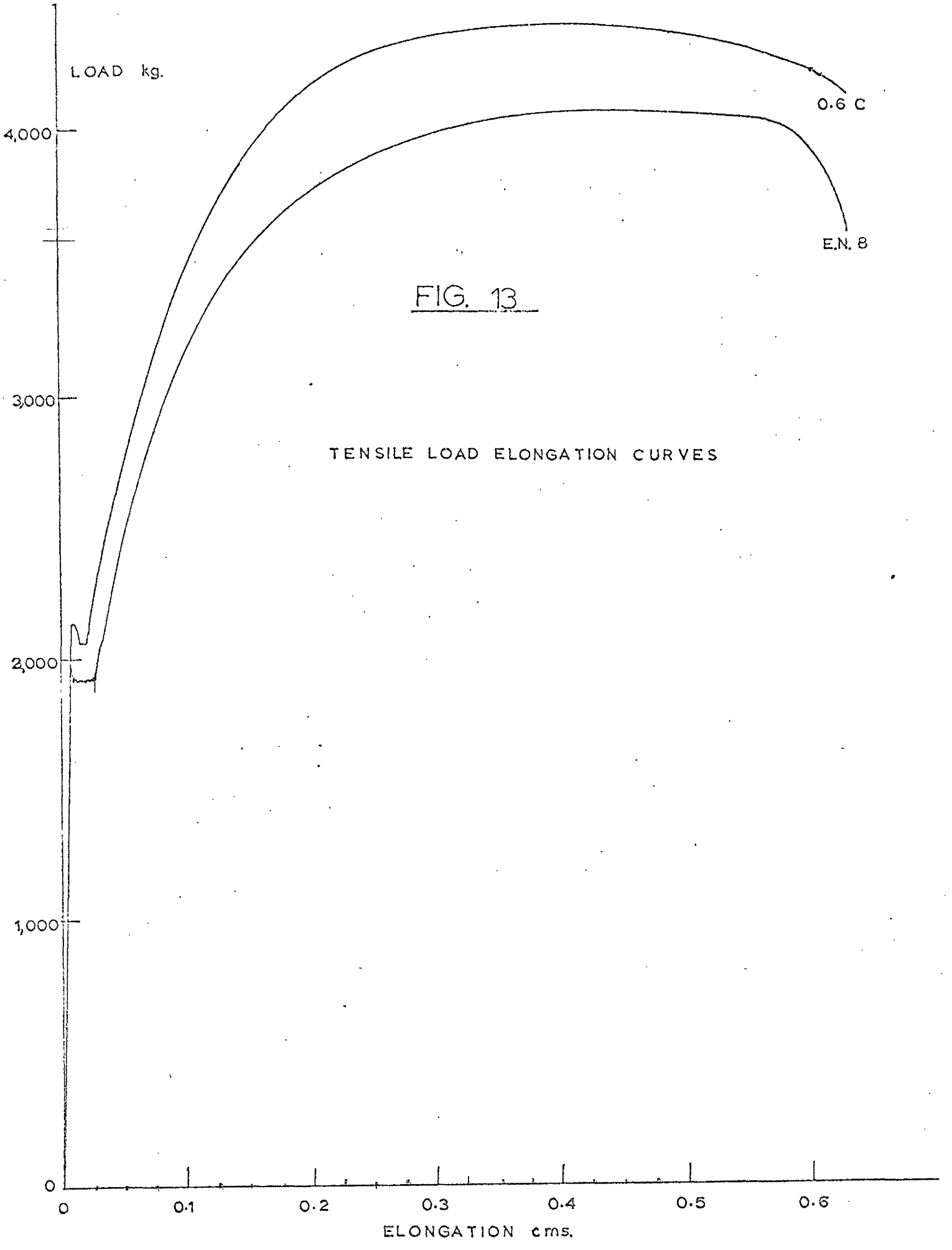

FIG. 13

TENSILE LOAD ELONGATION CURVES

Table 6

Tensile Test

Constraint Factor at centre of bar in necked region and maximum plastic deformation in the neck (see appendix 1)

Specimen	a cms.	R cms.	Constraint Factor
T 1	0.340	4.3	0.371
T 2	0.36	14.8	0.345
T 3	0.37	19.8	0.342
T 4	0.41	-	0.333

Specimen	Initial dia. cms.	Final dia. cms.	Plastic Strain $2 \ln (d_0 / d_f)$
T 1	0.875	0.68	0.508
T 2	0.882	0.72	0.414
T 3	0.882	0.74	0.348
T 4	0.882	0.82	0.154

Table 7

Tensile Test

Number of slip line defects in pearlite expressed as number per 0.01 mm^2

Specimen T1

Distance from Neck root mm.	No. of Defects	Average
0.0	14 ;11; 17; 12	13.5
1.0	10; 11; 10; 10	10.3
2.0	11; 9; 9; 10	9.8
3.0	12; 16; 9; 8	11.5
4.0	10; 9; 13; 10	10.3
6.0	12; 8; 13; 15	12.0
8.0	14; 7; 10; 11	10.5
Specimen T2		
0.0	11; 15; 9; 13	12.0
1.0	10; 12; 8; 7	9 .3
2.0	11; 11; 12; 8	10.5
3.0	9; 11; 10; 7	9.3
4.0	7; 13; 8; 10	9.5
5.0	9; 9; 12; 10	10.0
6.0	10; 10; 11; 14	11.3
7.0	9; 9; 8; 10	9.0
Specimen T4 (Strained to U.T.S. so no neck)		
	14; 11; 12; 14; 16 16; 11; 11; 12; 10	12.7

FIG: 14

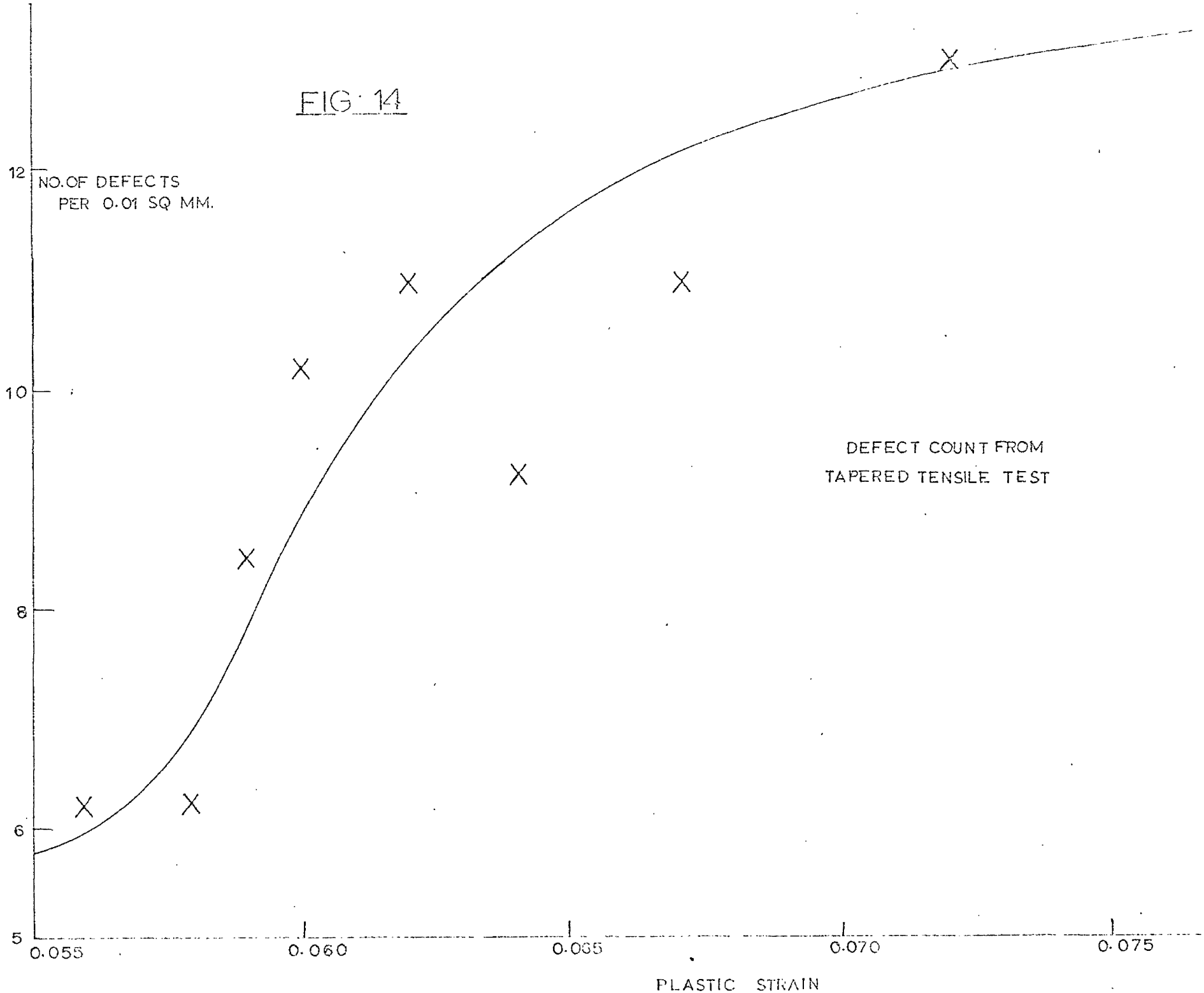
12
10
8
6
5
NO. OF DEFECTS
PER 0.01 SQ MM.
DEFECT COUNT FROM
TAPERED TENSILE TEST
0.055
0.060
0.065
0.070
0.075
PLASTIC STRAIN

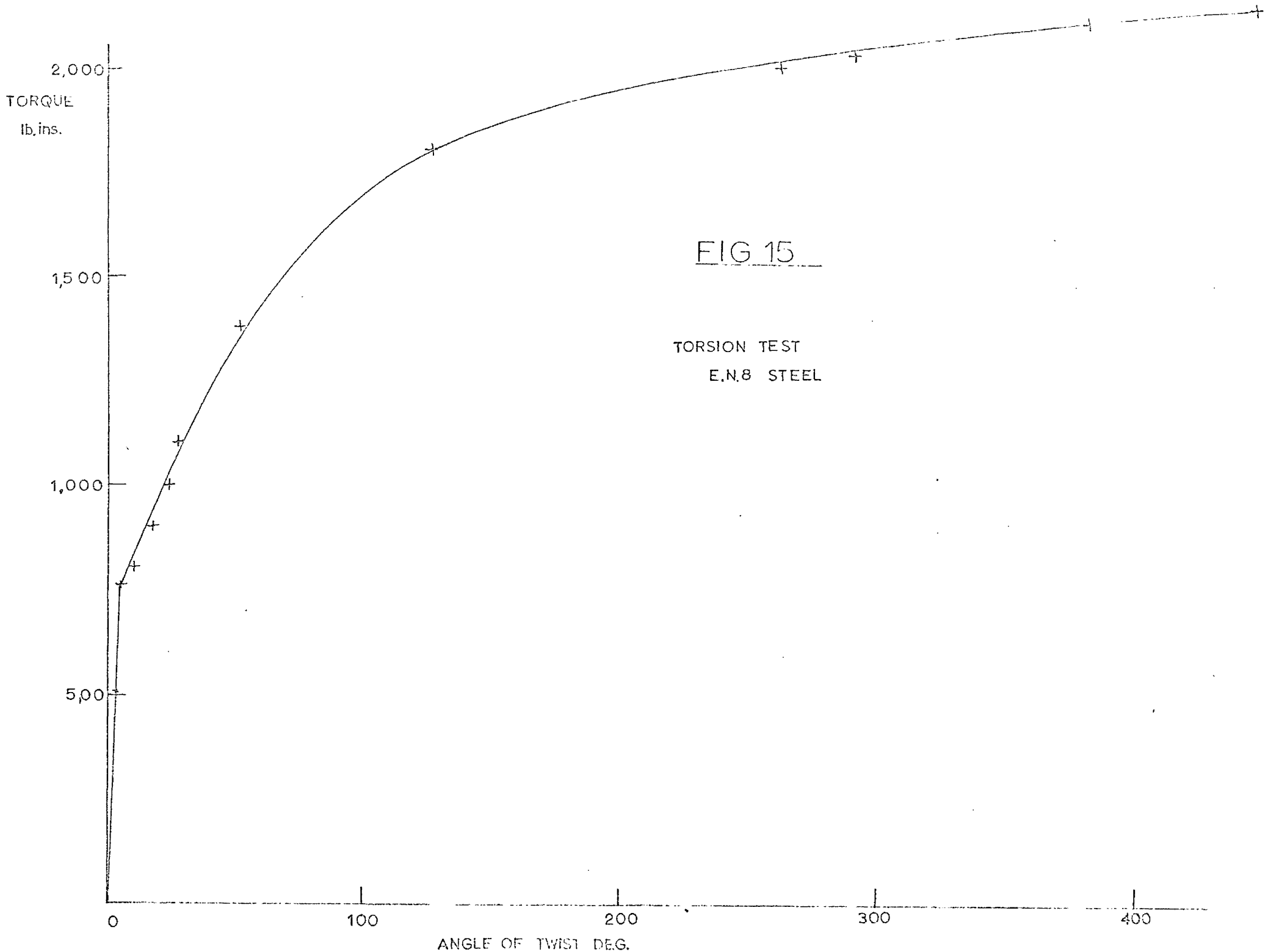

FIG 15

TORSION TEST
E.N.8 STEEL

Table 8

Torsion Test E.N.8 Specimen

Specimen Diameter = 0.5 ins.

Parallel length of specimen = 2.5 ins.

Angle to failure = 7.95 radians

Strain to failure from above data = 0.80

" " " " microstructure = 0.81

Shear strain at fracture from microstructure = 2.1

$$\text{Effective strain} = \frac{\text{Shear Strain}}{\sqrt{3}}$$

$$= \frac{2.10}{\sqrt{3}}$$

$$= 1.21$$

Fig. 16 X 500

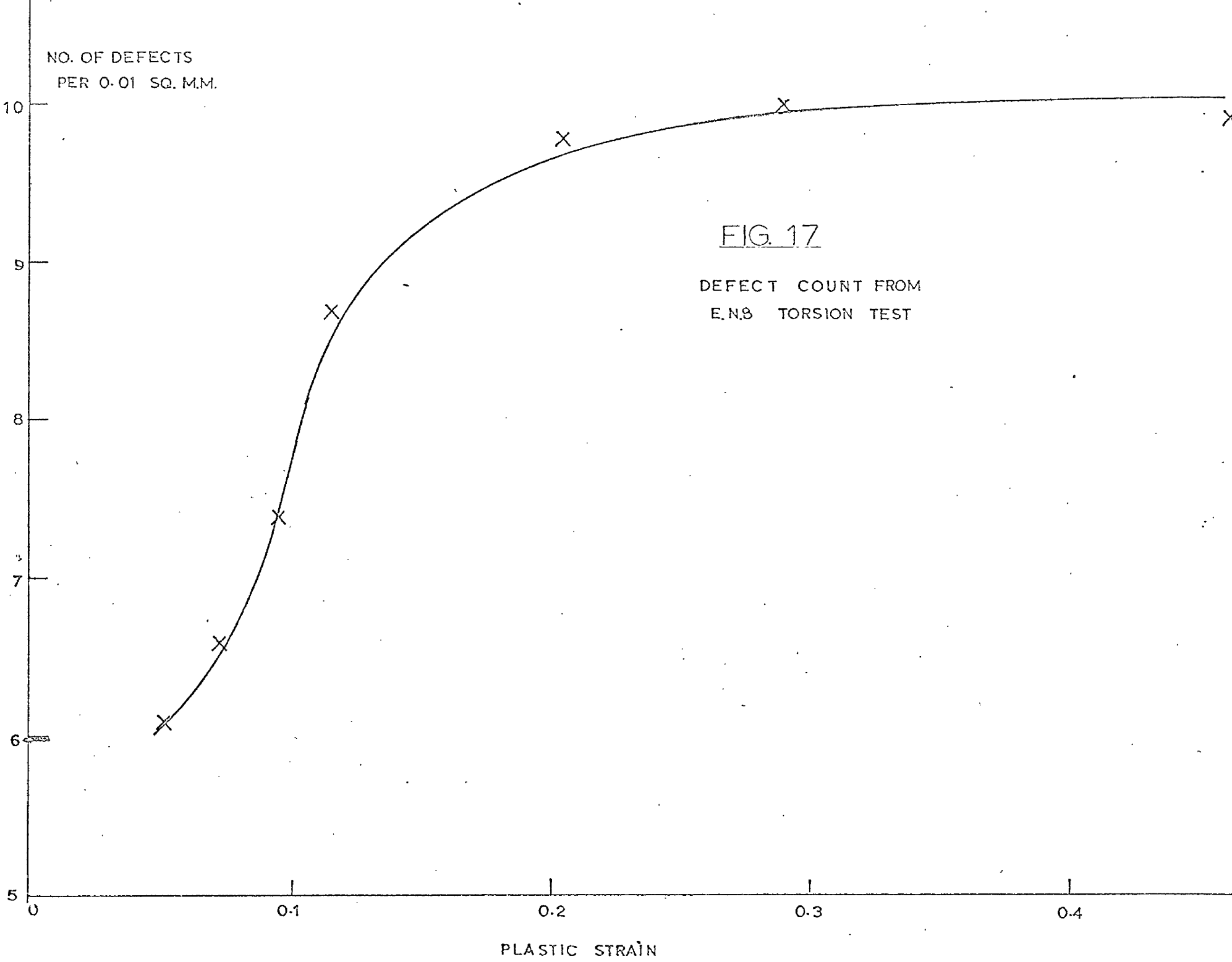

FIG. 17

DEFECT COUNT FROM
E.N.8 TORSION TEST

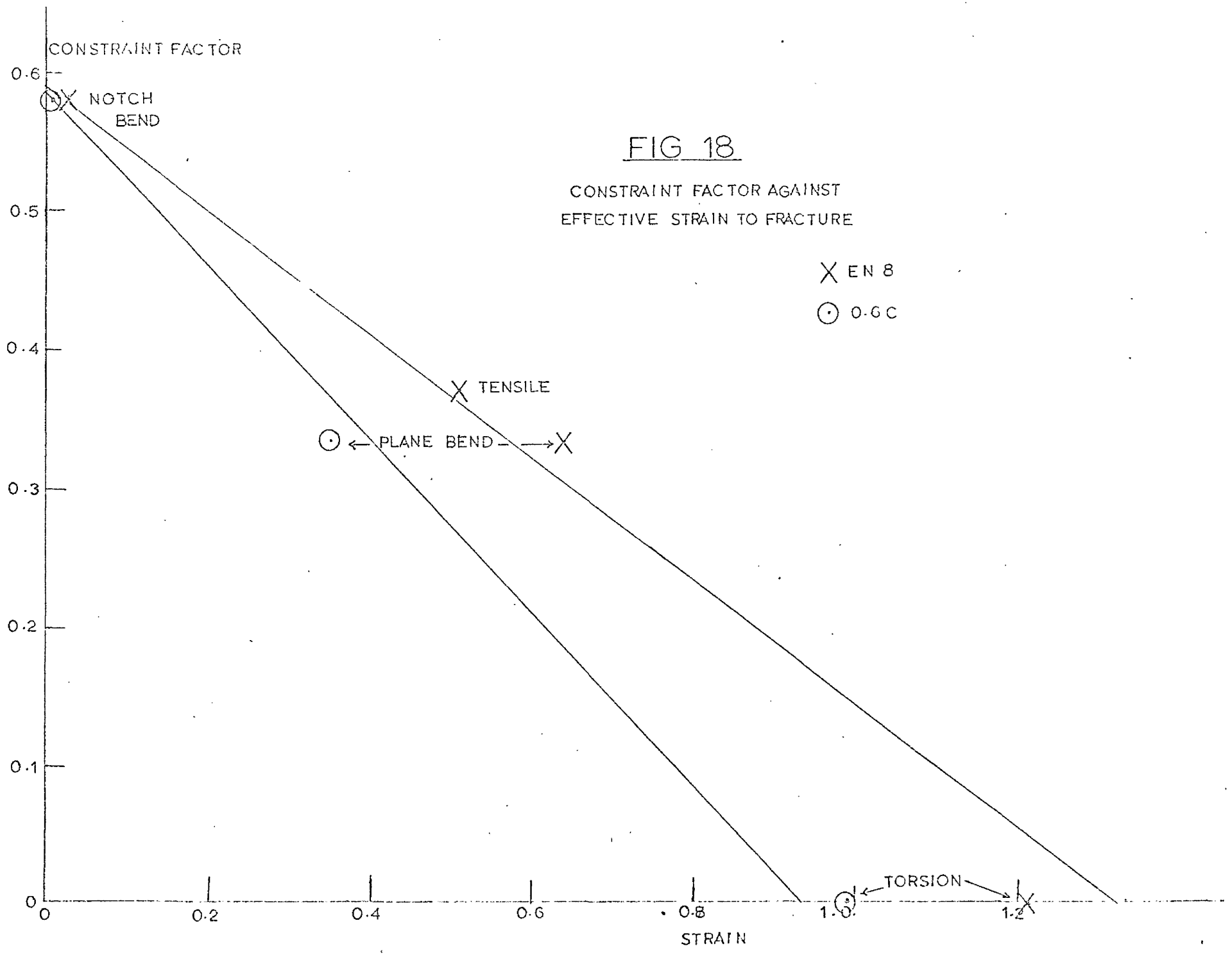

FIG 18

CONSTRAINT FACTOR AGAINST
EFFECTIVE STRAIN TO FRACTURE

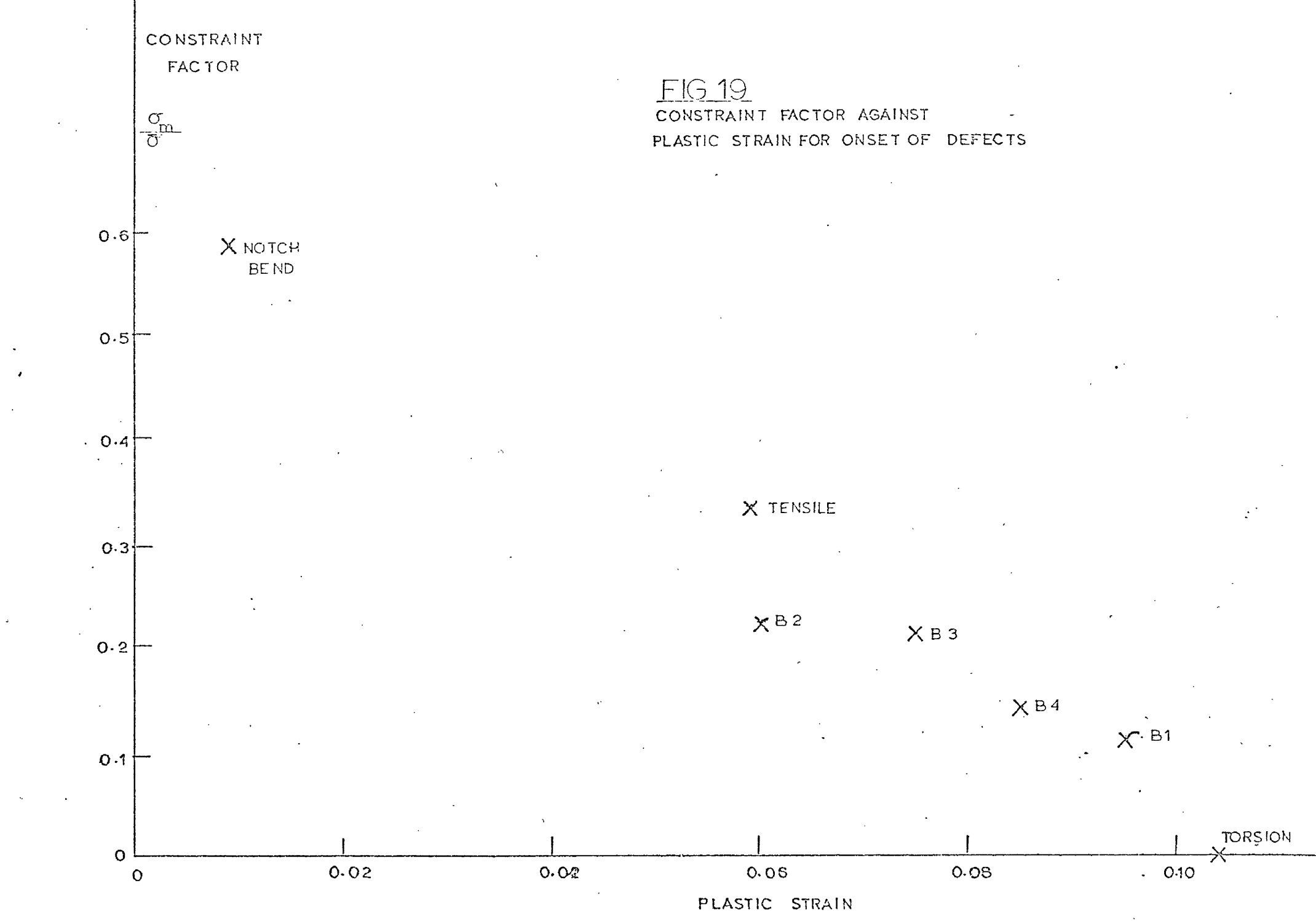

FIG 19

CONSTRAINT FACTOR AGAINST PLASTIC STRAIN FOR ONSET OF DEFECTS

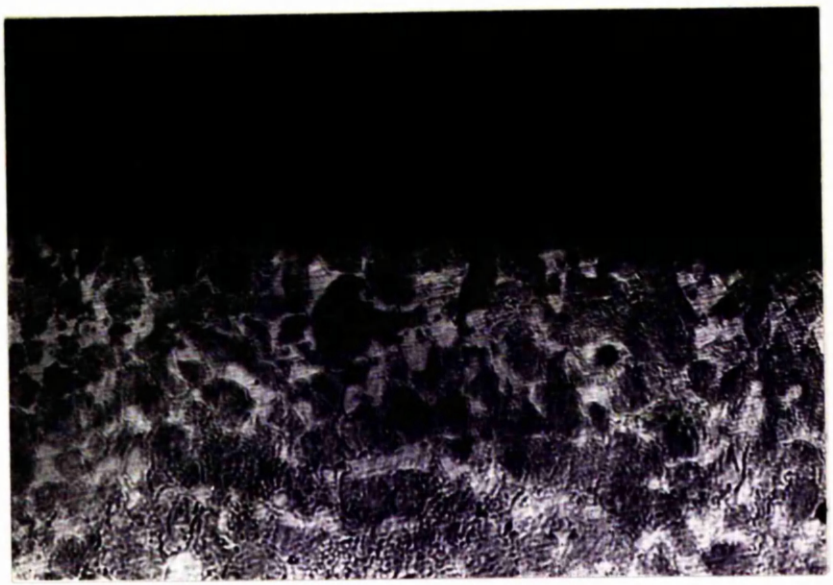

Fig. 20 X 100

Fig. 21 X 500

Fig. 22 X 500

Fig. 23 X 150

Fig. 24 X 500

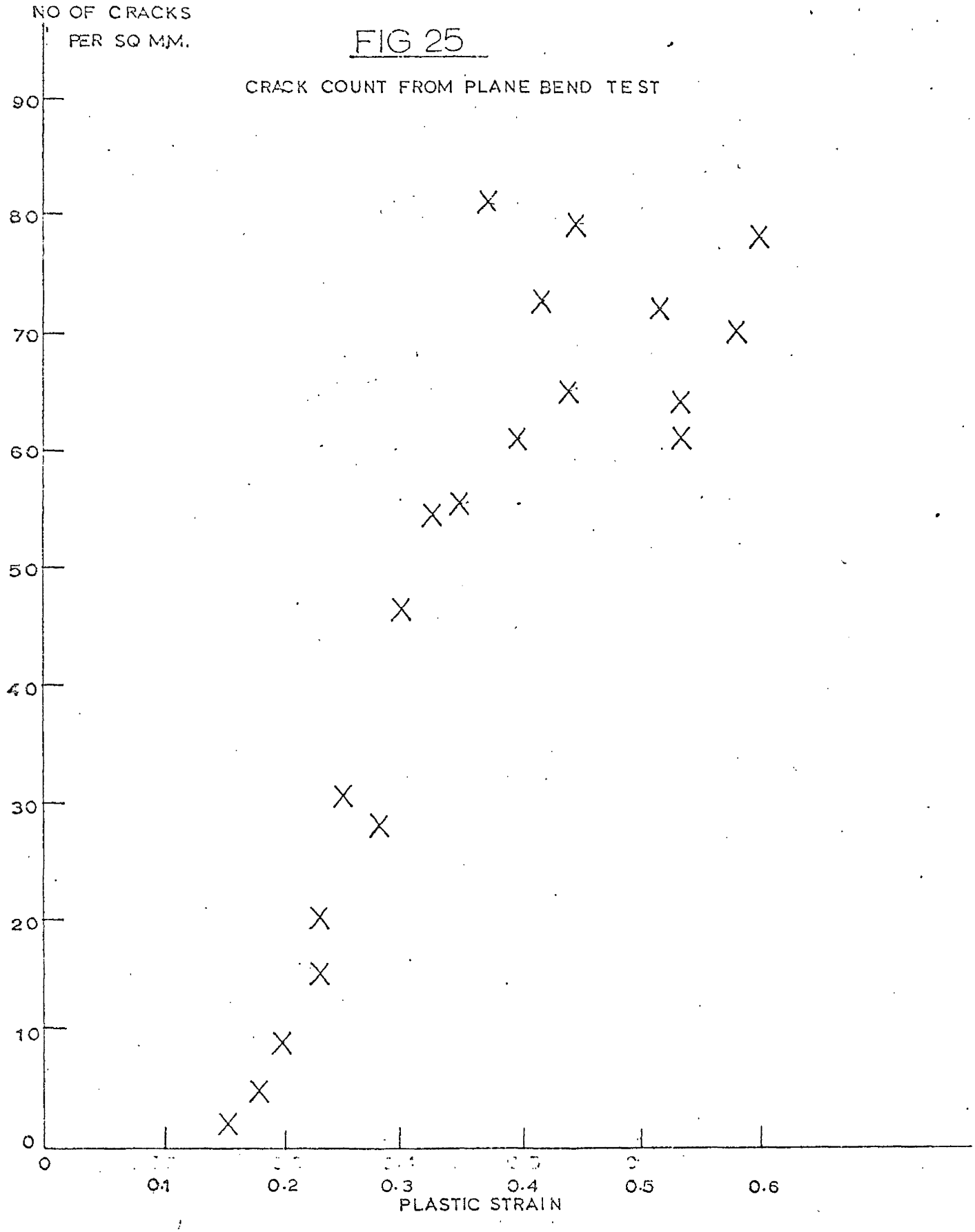
NO OF CRACKS
PER SQ MM.
FIG 25
CRACK COUNT FROM PLANE BEND TEST
90
80
70
60
50
40
30
20
10
0
0
0.1
0.2
0.3
0.4
0.5
0.6
PLASTIC STRAIN

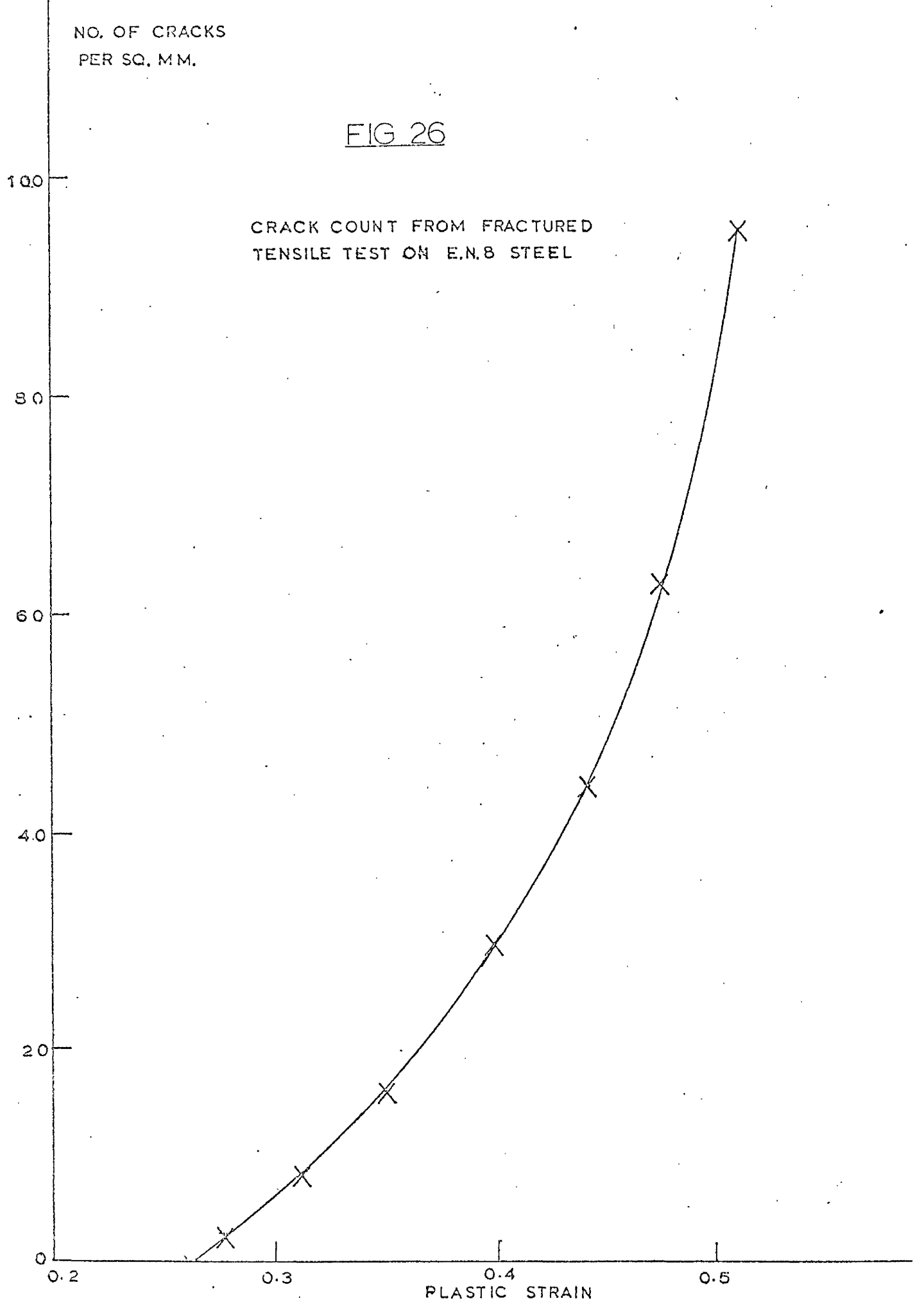

FIG 26

CRACK COUNT FROM FRACTURED
TENSILE TEST ON E.N.8 STEEL

Appendix 1

Correction for State of Stress in Neck of Tensile Specimen.

This analysis was carried out by Bridgmann (9) and is based on the observation that the axial strain component is constant across the neck.

From diagram C overleaf, R is the radius of the neck

a is the radius of the specimen in the necked region.

x is the distance from the centre of specimen

Bridgmann arrived at the relation:-

$$\frac{\sigma_{zz}}{\bar{\sigma}} = 1 + \ln\left[\frac{a}{2R} + 1 - \frac{x^2}{2aR}\right]$$

$$\sigma_{\theta\theta} = \sigma_{rr} = \sigma_{zz} - \bar{\sigma}$$

$\sigma_{\theta\theta}$, σ_{rr} & σ_{zz} are principal stresses

$\bar{\sigma}$ is the effective stress

In the centre of the bar, $x = 0$

$$\frac{\sigma_{zz}}{\bar{\sigma}} = 1 + \ln\left[\frac{a}{2R} + 1\right]$$

Constraint factor $$\frac{\sigma_m}{\bar{\sigma}} = \frac{\sigma_{\theta\theta} + \sigma_{rr} + \sigma_{zz}}{3\bar{\sigma}}$$

$$= \frac{2(\sigma_{zz} - \bar{\sigma}) + \sigma_{zz}}{3\bar{\sigma}}$$

$$= \frac{\sigma_{zz}}{\bar{\sigma}} - \frac{2}{3}$$

$$\frac{\sigma_m}{\bar{\sigma}} = 1 + \ln\left[\frac{a}{2R} + 1\right] - \frac{2}{3}$$

$$= \frac{1}{3} + \ln\left[\frac{a}{2R} + 1\right]$$

FIG. C

CO-ORDINATES OF NECKED TENSILE SPECIMEN

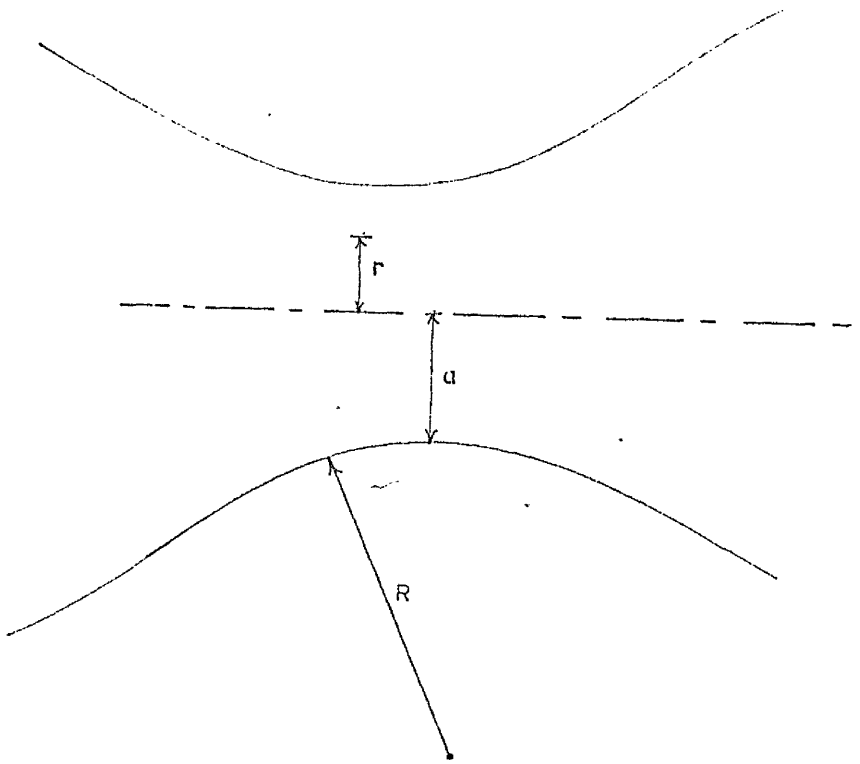

Appendix 2

Approximate Estimate of Strain in Notch Root

A solution to the problem of an unbounded elastic material containing two infinite hyperbolic notches is used. (Fig. A). The material is loaded in bending.

The foci of the notches are a distance 2c apart. This distance has been taken to be the approximate distance apart of the notch roots, i.e. for the specimens used in the tests, 2c is 1.9 cms.

Radius of Notch root is 0.02 cms.

y is the distance measured from the centre of the bar.

The stress on an element at y is σ_x given by:-

$$\sigma_x = \lambda \cos\eta\left(\frac{1}{\sin\eta} + \frac{\sin^2\eta_o}{\sin^3\eta}\right) \qquad \text{.... 1}$$ *

where in elliptical coordinates $y = c\cos\eta$

η = const. η_o, η_1, η_2 .... are hyperbolae

λ is a constant to be evaluated from the applied moment.

$$\text{root radius } x_o = c\,\frac{\sin^2\eta_o}{\cos\eta_o}$$

$$\text{giving} \qquad \eta_o = 0.145 = 8^\circ\ 18'$$

From 1 $\quad \sigma_x$ at notch root $= \lambda^2\,\frac{\cos\eta_o}{\sin\eta_o}$

$$= 13.7\,\lambda \qquad \text{..... 2}$$

* Neuber "Kerbspannungslehre" Springer Verlag 1937

Bending Moment $M = 2\int_{y=0}^{y=c} \sigma_x \, b \, y \, dy$

where $b = 2.54$ cms. and is the width of the bar.

when $y = 0$, $\eta = \pi/2$

and when $y = c$, $\eta = \eta_o$

$$M = 2b\int_{\pi/2}^{\eta_o} \lambda \cos\eta \left(\frac{1}{\sin\eta} + \frac{\sin^2\eta}{\sin^3\eta} \right) c \cos\eta (-c \sin\eta) d\eta$$

$$= -2bc^2\lambda \int_{\pi/2}^{\eta_o} \left[\cos^2\eta + \frac{\cos^2\eta}{\sin^2\eta} \sin^2\eta_o \right] d\eta$$

$$= \lambda \, bc^2 \left[\frac{\pi}{2} - \eta_o - \frac{1}{2} \sin 2\eta_o + 2 \sin^2\eta_o \left(\cot\eta_o - \frac{\pi}{2} + \eta_o \right) \right.$$

$$= \lambda \, 1.51 \, bc^2 \qquad \ldots\ldots 3$$

Thus from 2 & 3, $\sigma_x = 13.7 \dfrac{M}{1.51 \, b \, c^2}$

$$= 4M$$

Referring to the axes in fig. B, $\sigma_y = 0$

The stress/strain relations are:-

$$\varepsilon_x = \frac{1}{E} \left[\sigma_x - \nu\sigma_z \right]$$

$$\varepsilon_y = \frac{1}{E} \left[0 - \nu (\sigma_x + \sigma_z) \right]$$

$$\varepsilon_z = \frac{1}{E} \left[\sigma_z - \nu\sigma_x \right]$$

Taking $\varepsilon_z \simeq 0$ for plane strain conditions at the

centre of the notch and ν, Poisson's ratio = 0.3 gives

$$\sigma_z = -0.3\,\sigma_x$$

$$\varepsilon_x = \frac{\sigma_x}{E}\left[1 - 0.09\right]$$

$$\varepsilon_y = \frac{\sigma_y}{E}\left[0.3 + 0.09\right]$$

$$\bar{\varepsilon}^p = \sqrt{\frac{2}{9}\left(\varepsilon_x - \varepsilon_y\right)^2 + \varepsilon_x^2 + \varepsilon_y^2}$$

$$= \frac{\sigma_x}{E}\sqrt{\frac{2}{9}\left(1.3^2 + 0.91^2 + 0.39^2\right)}$$

$$= \frac{\sigma_x}{E}\sqrt{0.56}$$

$$= \frac{0.77\,\sigma_x}{E}$$

$$= \frac{3.1\,M}{E}$$

$E = 2 \times 10^6$ kg./cm^2

For B.H.8 specimen M4, M = 15,000 kg.cm

$$\bar{\varepsilon}^p = 0.023$$

For 0.6C steel, bending moment to fracture = 13,500 kg.cm. assuming elastic conditions only.

$$\bar{\varepsilon}^p = 0.02$$

The value for the 0.6C steel does not take into account any cracking before complete failure.